molecular pharmaceutics

Review

pubs.acs.org/molecularpharmaceutics

Positron Emission Tomography Image-Guided Drug Delivery: Current Status and Future Perspectives

Rubel Chakravarty,*[,†,‡] Hao Hong,[†] and Weibo Cai*[,†,§,∥]

[†]Department of Radiology, University of Wisconsin—Madison, Madison, Wisconsin 53705-2275, United States
[‡]Isotope Applications and Radiopharmaceuticals Division, Bhabha Atomic Research Centre, Mumbai 400085, India
[§]Department of Medical Physics, University of Wisconsin—Madison, Madison, Wisconsin 53705-2275, United States
[∥]University of Wisconsin Carbone Cancer Center, Madison, Wisconsin 53705-2275, United States

ABSTRACT: Positron emission tomography (PET) is an important modality in the field of molecular imaging, which is gradually impacting patient care by providing safe, fast, and reliable techniques that help to alter the course of patient care by revealing invasive, de facto procedures to be unnecessary or rendering them obsolete. Also, PET provides a key connection between the molecular mechanisms involved in the pathophysiology of disease and the according targeted therapies. Recently, PET imaging is also gaining ground in the field of drug delivery. Current drug delivery research is focused on developing novel drug delivery systems with emphasis on precise targeting, accurate dose delivery, and minimal toxicity in order to achieve maximum therapeutic efficacy. At the intersection between PET imaging and controlled drug delivery, interest has grown in combining both these paradigms into clinically effective formulations. PET image-guided drug delivery has great potential to revolutionize patient care by *in vivo* assessment of drug biodistribution and accumulation at the target site and real-time monitoring of the therapeutic outcome. The expected end point of this approach is to provide fundamental support for the optimization of innovative diagnostic and therapeutic strategies that could contribute to emerging concepts in the field of "personalized medicine". This review focuses on the recent developments in PET image-guided drug delivery and discusses intriguing opportunities for future development. The preclinical data reported to date are quite promising, and it is evident that such strategies in cancer management hold promise for clinically translatable advances that can positively impact the overall diagnostic and therapeutic processes and result in enhanced quality of life for cancer patients.

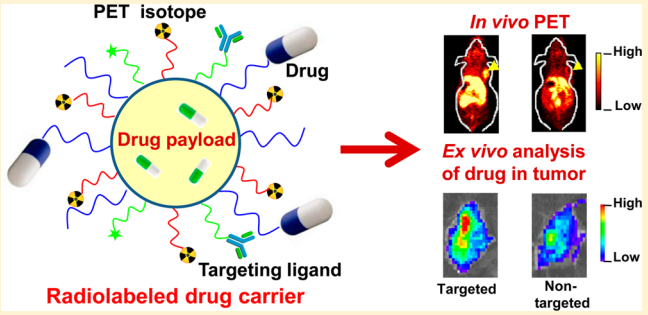

KEYWORDS: *positron emission tomography, image-guided drug delivery, cancer, theranostics, molecular imaging, personalized medicine*

INTRODUCTION

Targeted drug delivery guided by molecular imaging approaches is a burgeoning area of clinical research, particularly for the treatment of cancer.[1−5] This approach involves an optimized delivery of a therapeutic molecule and an imaging probe to the disease site, thereby using selective diagnosis and effective pharmacotherapy in unison for management of several diseases. Successful utilization of this strategy requires integrated knowledge and versatile approaches in multidisciplinary fields such as cell and molecular biology, chemistry, material science, and physics and has opened up vast prospects in pharmacokinetics, therapeutic target discovery, drug delivery research, and quantification of multiple biomarkers in diseases. The major goal of this approach is to use molecular imaging to maximize effective therapy in diseased tissues and to minimize systemic drug exposure in order to reduce toxicities. In the past decade, innumerable studies have been reported on the synergistic use of molecular imaging with targeted drug delivery, and this strategy has now matured with promises to fulfill the vision of "personalized" medical treatment in the near future.[5−9]

In order to minimize the effects of toxicity and improve therapeutic effects, it is essential to deliver the therapeutic drugs to the right site, in the right time, and in the right concentration. Ideally, the drug should act as a "magic bullet" that possesses perfect specificity to targeted lesions and has no side effect on the rest of the body. Controllable and selective delivery of drugs improves bioavailability by preventing premature degradation and enhancing uptake, maintains drug concentration within the therapeutic window by adjusting the drug release rate, and reduces side effects by targeting to disease site and target cells.[1,10] The ability to deliver therapeutic drugs

Special Issue: Positron Emission Tomography: State of the Art

Received: March 3, 2014
Revised: May 23, 2014
Accepted: May 27, 2014
Published: May 27, 2014

locally, in a minimally invasive manner, has advanced drastically with the growth of molecular imaging techniques.[11−17] Molecular imaging approaches have been implemented in areas ranging from new therapeutic target discovery to effectively monitoring tumor pharmacokinetics and drug distribution to modulation of drug release at the target site.[1,4,6,18] When molecular imaging probes are coadministered as part of the drug delivery system, it can help to achieve multiple goals, such as real-time and concurrent assessment of drug delivery efficiency/targeting, *in vivo* fate of drug and sites of localization/accumulation, modes of excretion, imaging, and monitoring the progress of drug treatment, in a single dosing. When an image-guided approach is not used, there is neither any means to track or image the *in vivo* fate nor the ability to measure the delivery efficiency of drugs. Also, the bioavailability, therapeutic efficacy, and dose response of drug treatment has to be estimated based on separate sets of experiments which might render the process cumbersome and cost-ineffective. However, molecular imaging of the drug delivery process involves several challenges and is affected by several factors such as target expression, type of drug, *in vivo* accessibility of the receptor (e.g., vascular density, vascular permeability, and interstitial pressure), enhanced permeability and retention (EPR) effect, receptor internalization, tracer protein dose, and timing of imaging.[4,6,7,10,11] Nevertheless, this approach has the potential for patient selection for targeted therapy and monitoring the therapeutic response after the drug is delivered.

Currently, several noninvasive image-guided modalities are being used in biomedical and clinical settings, which include magnetic resonance imaging (MRI), computed tomography (CT), positron emission tomography (PET), single photon emission computed tomography (SPECT), optical imaging, and ultrasonography.[14,16,19−21] Among these, PET, SPECT, and optical imaging are regarded as quantitative or semi-quantitative imaging modalities, whereas CT and MRI are normally used for anatomical imaging. The relative advantages and limitations of these imaging modalities have been elaborately discussed in several review articles.[14,16,19−21] In particular, PET offers picomolar sensitivity and is a fully translational noninvasive functional imaging technique with high sensitivity and accurate quantification and thus helps in measuring biological processes at the molecular and the metabolic levels *in vivo*. However, the limited spatial resolution of the PET images might sometimes make it difficult to accurately define the regions of interest (ROIs).[19] Unnecessary radiation exposure to the nontargeted organs due to highly energetic γ-rays (511 keV) emitted by the PET radioisotopes is also a cause of concern. Nevertheless, one has to acknowledge that no single imaging modality can provide information on all aspects of structure and function. Therefore, investigation of a subject using multiple imaging modalities is highly desirable and is rapidly gaining popularity.[20−23]

In this review, we aim to provide a timely and comprehensive overview of the PET image-guided drug delivery approaches reported to date, with focus on quantitative assessments of tumor-targeted therapeutic delivery, distribution, uptake, and response. The development of various carriers for site- and event-specific targeting and controlled drug release are summarized, and the great potential and intriguing opportunities for future development which might help in bringing this exciting research avenue closer to a clinical reality are discussed.

■ PET IMAGING

The interest in using PET as a molecular imaging modality in clinical research has steadily grown during the last 2−3 decades, and has now gained considerable importance in routine hospital practices because of its ability to diagnose diseases in early stages and monitor therapeutic responses.[13,19,24−27] In a typical scenario of PET imaging, a suitable compound is radiolabeled with positron-emitting radionuclides such as ^{18}F, ^{64}Cu, ^{68}Ga, or ^{89}Zr and administered to a living subject.[19] The positron that emerges from the radionuclide decay travels a short distance before being annihilated with an electron to release two 511 keV γ rays, which are approximately 180° apart. The 511 keV γ rays can be detected by a ring of detectors configured in the coincidence mode in the PET camera. The registered events are reconstructed into a three-dimensional image which provides information on the spatial distribution of the radioactivity as a function of time in the living subject.[19] Nowadays, PET is increasingly used in combination with CT as a hybrid imaging modality in clinical settings, to obtain higher resolution by fusing both functional and anatomical information at the same time.

PET also plays an important role in the process of drug development and evaluation, whereby understanding drug action and establishing dosage regimens and treatment strategies have been most crucial.[28−32] Positron-emitting radionuclides of elements such as C, N, O can replace the stable analogues in drugs and biomolecules, and hence it is possible to synthesize PET probes with the same chemical structure as the parent unlabeled molecules without altering their biological activity. Low bioavailability, insufficient targeting, and poor localization in desired tissue/organ, adverse side effects, etc. are some of major concerns with most of the systemic drug delivery approaches.[10] Targeted drug delivery systems have the potential to improve these undesirable features, and when used in conjunction with PET imaging, they are effective in increasing safety to efficacy ratio and decreasing dose, which in turn reduces adverse reactions and toxicity of drugs. PET can also provide information on the kinetics, dosimetry, and distribution of drugs in the diseased and normal tissues within the field of view as well as the clearance pattern in a biological system.

PET image-guided drug delivery is expected to play an increasingly important role in realizing the full potential of the next generation of therapeutics. For this purpose, it is essential to choose radioisotopes of appropriate half-lives to match the pharmacokinetics of the drug carriers used. Generally, for inorganic drug carriers (such as silica nanoparticles, superparamagnetic iron oxide nanoparticle, gold nanoparticles, quantum dots etc.) which are expected to have circulation half-lives of a few hours,[33−36] short-lived or intermediate-lived radioisotopes such as ^{68}Ga ($t_{1/2}$ = 68 min), ^{18}F ($t_{1/2}$ = 109.8 min), ^{44}Sc ($t_{1/2}$ = 3.9 h), ^{66}Ga ($t_{1/2}$ = 9.7 h), ^{64}Cu ($t_{1/2}$ = 12.7 h), etc. are more suitable. However, for organic drug carriers (such as carbon nanotubes, polymeric nanoparticles, micelles, liposomes, etc.), which can circulate *in vivo* for more than 1 day,[37−39] intermediate-lived or long-lived radioisotopes such as ^{66}Ga ($t_{1/2}$ = 9.7 h), ^{64}Cu ($t_{1/2}$ = 12.7 h), ^{89}Zr ($t_{1/2}$ = 78.4 h), or ^{124}I ($t_{1/2}$ = 4.17 day) would be the ideal choices for PET image-guided drug delivery. The choice of suitable radioisotopes is also governed by the conjugation strategies adopted for radiolabeling the drug carrier. The radiolabeled agent must

Table 1. Representative Examples of Different Drug Delivery Systems That Were Radiolabeled with Different Positron Emitter Radionuclides for PET Image-Guided Drug Delivery Applications

drug carrier	targeting ligand	target	therapeutic agent	PET isotope	disease model	tumor uptake	ref
albumin	anti-VEGFR2-antibody	vascular endothelial growth factor receptor 2	None	^{18}F	human breast cancer	~ 1% ID/g	56
liposome	none (passive targeting)	none (passive targeting)	model hydrophilic drug	^{18}F and ^{64}Cu	Met-1 tumors	*a*	75
micelles	cRGD peptide	integrin $\alpha_v\beta_3$	doxorubicin	^{64}Cu	human glioblastoma	~7% ID/g	86
enzyme/prodrug	AADC tracer, 6-[^{18}F] fluoro-L-mtyrosine (FMT)	transgene expression in brain	L-amino acid decarboxylase (AADC) gene and a prodrug, dopamine	^{18}F	Parkinson's disease	*a*	97
gold nanorods	cRGD peptide	integrin $\alpha_v\beta_3$	doxorubicin	^{64}Cu	human glioblastoma	~ 6% ID/g	132
mesoporous silica nanoparticles	TRC105 antibody	CD105	doxorubicin	^{64}Cu	murine breast cancer	~6% ID/g	142
poly(lactide-coglycolide) nanoparticles	none (passive targeting)	none (passive targeting)	dithiazanine iodide	^{18}F	human glioblastoma	*a*	157
nanographene oxide	TRC105 antibody	CD105	doxorubicin	^{64}Cu	murine breast cancer	~6% ID/g	167
conventional radiopharmaceutical (^{68}Ga-DOTATATE)	peptide octreotate (TATE)	somatostatin receptor	^{177}Lu-DOTATATE	^{68}Ga	neuroblastoma		190,191

[a]Not reported.

demonstrate high *in vitro* and well as *in vivo* stability for successful use in PET image-guided drug delivery.

CARRIERS FOR PET IMAGE-GUIDED DRUG DELIVERY

The current revolution in targeted drug delivery is fueled by the innovations in material science, organic chemistry, functional genomics, and proteomics which have created carriers that are biodegradable (which can be slowly dissolved *in vivo* by biological means), biocompatible (which can remain in a biological system without causing any adverse effect), targeting, and stimulus-responsive (which can control drug biodistribution in response to specific stimuli).[10] In addition to increased selectivity against diseased cells, these delivery systems can also solve problems associated with drug instability in the biological environment as well as issues related to the modulation of drug. Two different approaches are used for drug loading and delivery for pinpoint targeted treatment of cancer cells. In the first approach, chemotherapeutic drugs are loaded onto multifunctional drug carriers such as liposomes, micelles, nanoparticles, microparticles, microbubbles, dendrimers, copolymers, intestinal pathogen, etc.[9,40,41] Owing to the convenience in modifying the surface properties of these carrier systems, they can be conjugated with various targeting ligands such as monoclonal antibodies, antibody fragments, peptides, and other small molecules.[9,40,41] The carriers are either directly conjugated to targeting ligands or derivatized for interactions with specific adapters that are conjugated to the targeting vectors. Streptavidin/biotin interaction is one good example used for binding various carriers to targeting proteins and antibodies.[42] In addition to delivery of chemotherapeutic drug molecules for therapy, these carriers also carry PET radionuclides or other contrast agents for diagnosis of the diseases. Such drug delivery strategies are an important move toward achieving simultaneous diagnosis and therapy of diseases, which have recently been termed as "theranostics".[9,43]

In the second approach, drugs (e.g., therapeutic radionuclides) are conjugated with the targeting ligands using suitable bifunctional linkers.[9,44] Unlike the first approach, here the drug and the imaging label (PET radionuclide) do not necessarily share the same delivery carrier. For diagnosis or monitoring therapeutic response, PET imaging is carried out separately in this case by conjugation of the targeting ligands with suitable PET radioisotopes. Another striking difference between the two approaches is that, in the former, the delivery of the drug to the target tissue can be achieved by both passive and active targeting, while, in the latter, the drug is delivered primarily due to active targeting.[45] In passive targeting, the drug carriers such as nanoparticles, liposomes, micelles, etc. can reach the tumor sites through the EPR effect.[45] Also, therapeutic concentrations can be much lower than optimal at the tumor site by simply relying on EPR-mediated accumulation, and therefore passive targeting is generally not preferred for drug delivery. More efficient and selective uptake of drug into the target cells is achieved by active targeting wherein the drug carriers are conjugated with targeting ligands, as mentioned earlier. Active targeting requires careful identification of tumor biomarkers, as well as selection of specific molecules that can bind to such markers in a selective and directed manner. Targeted drug delivery vehicles can then be internalized by tumor cells via receptor-mediated endocytosis/phagocytosis, resulting in elevated concentration of drugs in tumor tissue.

Thus, the concept of "theranostic agent" is not just limited to chemotherapy but also has a relevant role to guide in radiation-based targeted therapies. Various drug carrier systems have been radiolabeled with different positron emitter radionuclides for image-guided drug delivery, most of which are summarized in Table 1 and discussed in the following text.

Albumin-Based Delivery Approach. Albumin is an attractive macromolecular carrier that may be modified suitably for biomedical imaging applications.[46] Such carriers have also been studied for drug and gene delivery *in vitro* and *in vivo*, through cavitation.[47−49] Generally, albumin-based carriers are biodegradable, nontoxic, metabolized *in vivo* to produce harmless degradation products, nonimmunogenic, easy to purify, and soluble in water allowing ease of delivery by

injection and thus ideal candidates for image-guided drug delivery procedures. A significant amount of drug can be incorporated in the albumin based carrier systems because of different binding sites present in the albumin molecule. Owing to the defined albumin primary structure and high content of charged amino acids (e.g., lysine) on the surface, albumin-based carriers offer the possibility of direct electrostatic adsorption of positively (e.g., ganciclovir) or negatively charged (e.g., oligonucleotide) molecules without the requirement of any other compound.[47] In addition, these carriers can easily be prepared under mild conditions by coacervation, controlled desolvation, or emulsion formation.[47] Commercially, albumins are obtained with significant quantities from egg white (ovalbumin), bovine serum (bovine serum albumin, BSA), and human serum (human serum albumin, HSA) and also available from soybeans, milk, and grains.[47]

The chelator-free radiolabeling of macroaggregated human serum albumin with ^{68}Ga ($t_{1/2}$ = 68 min) for PET imaging was first described by Even et al.[50] Subsequently, this procedure was improved, and development of a kit for labeling macroaggregated human serum albumin with ^{68}Ga for PET imaging of liver anomalies was reported by Okada et al.[51] The kit was clinically tested and was found useful in the evaluation of the function of the reticuloendothelial system. In a similar study, Maus et al. reported the radiolabeling of different commercially available human serum albumin kits with ^{68}Ga.[52] *In vivo* PET imaging showed that ^{68}Ga-labeled human serum albumin was mainly retained in the lungs. No decrease in activity or migration of particles from the lungs was observed during the first 1 h (~1 half-life of ^{68}Ga), which demonstrated the *in vivo* stability of the radiolabeled albumin over that period of time. Also, no significant retention of ^{68}Ga-labeled human serum albumin particles in the liver was detected. The authors concluded that this approach could be used to estimate the liver-to-lung shunt and eliminate extrahepatic macroaggregate deposition in patients with primary and secondary liver malignancies, warranting ^{90}Y-based radioembolization therapy.[53−55]

In a recent development, Liao et al. prepared albumin shelled microbubbles filled with perfluorocarbon (C_3F_8) gas to enhance the contrast in ultrasound imaging.[56] Additionally, the microbubbles were radiolabeled with *N*-succinimidyl-4-[^{18}F]-fluorobenzoate (^{18}F-SFB) and also conjugated with antibodies targeting vascular endothelial growth factor receptor 2 (VEGFR2) using avidin−biotin interaction. The radiolabeled microbubble shells could thus be used as dual-modality (PET and ultrasound) imaging agent. The ^{18}F-labeled, albumin-shelled, VEGFR2-targeted microbubbles had a lifetime of 30 min in the blood pool and demonstrated a highly specific adherence to tumor vessels in mice bearing human breast cancer. The size of the microbubbles was on the order of several micrometers and therefore should be retained in the tumor vasculature after intravenous injection. However, dynamic microPET imaging showed a relatively low tumor uptake of ~1% ID/g, even 1 h post injection. The low tumor uptake might be attributed to attachment of ^{18}F-SFB on the surface of the microbubble, which might have influenced the targeting efficiency of the antibody. The targeted microbubbles accumulated rapidly in both the liver and lung and cleared slowly from the blood circulation. The trends found in microPET imaging were further corroborated by *ex vivo* biodistribution studies. The specificity of the binding of targeted microbubbles to endothelial VEGFR2 was further validated by comparing the results of targeted and nontargeted contrast-enhanced ultrasound imaging. The authors concluded that the ^{18}F-labeled albumin-shelled microbubbles can be used for targeted drug delivery to VEGFR2 in breast cancer, guided by the dual-modality (PET/ultrasound) functional imaging approach.

In all these studies, development of only imaging strategies using albumin-based platforms have been described without direct relation to drug delivery. However, there are several other reports on utility of drug-loaded albumin-based carriers and controlling drug release using ultrasound energy in such systems.[47] Therefore, it was expected that tracking disease progression would be analogous to tracking drug delivery using albumin-based carriers. This hypothesis might also be valid for other drug carrier systems described below.

Liposome-Based Delivery Approach. Liposomes are concentric, closed bilayer membranes of water-insoluble polar lipids that can that can be used to encapsulate biomolecules and drugs for targeted delivery while protecting their bioactivity. Soluble drugs can be loaded in the aqueous core and the hydrophobic drugs partitioned in the lipid bilayer. Liposomal carriers are the earliest and the most extensively studied drug delivery carriers.[57−59] They are widely used not only in delivery of a variety of anticancer drugs but also in delivery of antineoplastic agents, antimicrobial compounds, immunomodulators, anti-inflammatory agents, cardiovascular drugs, etc.[57,58] The widespread interest in the use of liposomal systems for drug delivery stems from their biocompatibility, biodegradability, and nontoxicity and the ease of controlling their size during the preparation process. Currently, there are several commercially available liposomal formulations for cancer therapy, including doxorubicin (Doxil), daunorubicin (Daunoxome), cytarabine (Depocyt), Myocet, and vincristine (ONCO-TCS).[57,58] Many liposomal-based drug delivery systems are currently undergoing global clinical trials.[57,58] The recent advances in the use of radiolabeled liposomes for imaging as a tool in personalized medicine have been summarized in a recent review.[59]

Generally, liposomal systems are coated with poly(ethylene glycol) (PEG) to increase the circulation time in blood and decrease uptake in the reticuloendothelial system (RES).[60−62] Radiolabeling of liposomes with PET radioisotopes generally requires the use of chelator molecules in the aqueous core or conjugation on the lipid bilayer. The radiolabeled liposomal systems employed in PET studies must be carefully designed as lower stability of radiolabeled agent might obscure image-based assessment of particle pharmacokinetics. Seo et al. reported the development of a method for radiolabeling liposomes with ^{64}Cu for imaging and drug delivery monitoring using PET.[63,64] Bifunctional chelators, such as, 6-[*p*-(bromoacetamido)benzyl]-1,4,8,11-tetraazacyclotetradecane-*N*,*N*′,*N*″,*N*‴-tetraacetic acid (BAT), (6-(6-(3-(2-pyridyldithio)propionamido)hexanamido)-benzyl)-1,4,8,11-tetraazacyclotetradecane-1,4,8,11-tetraacetic acid (TETA-PDP), and 4-(2-(2-pyridyldithioethyl)-ethanamido)-11-carboxymethyl-1,4,8,11-tetraazabicyclo(6.6.2)-hexadecane (CB-TE2A-PDEA) were radiolabeled with ^{64}Cu, and the radiolabeled conjugates were attached to maleimide lipids in the liposome. The radiolabeled liposomes were found to be stable in mouse serum even after 48 h of incubation. *In vivo* PET studies demonstrated that liposomal activity was high in the blood pool from 0 to 6 h and slowly cleared out through the RES. The presence of the PEG spacer between the chelator and the lipid did not significantly alter the labeling efficiency

and the clearance rate of liposomes from the blood pool. The study was further extended by the same group of authors to characterize the *in vivo* clearance of ^{64}Cu-labeled distearoyl and dipalmitoyl lipids included within PEGylated liposomes.[65] *In vivo* PET imaging studies established that changes in lipidacyl chain length can result in desorption of lipid from the liposomal anchorage and interaction with blood components. Therefore, this factor should be considered for liposomal PET studies as desorption can rapidly alter the apparent pharmacokinetics.

In another study, Peterson et al. developed a remote loading method using 2-hydroxyquinoline ionophore, to carry ^{64}Cu across the membrane of preformed liposomes and deliver it to an encapsulated copper-chelator.[66] A highly efficient loading (>95%) and retention stability (>99%) was obtained adopting this approach. *In vivo* PET imaging studies demonstrated that a maximum tumor uptake of ∼5% ID/g with high tumor to muscle ratio could be achieved. The ^{64}Cu-liposomes reached a maximum level in the liver and spleen after 4 h and subsequently remained at a constant level. Also, the ^{64}Cu-liposomes remained in the blood pool for >24 h. The method provided ^{64}Cu-labeled liposomes with excellent imaging properties due to the high concentration of ^{64}Cu inside the liposomes and restricted exchange of ^{64}Cu with the biological environment due to the protective barrier constituted by the liposomal membrane. The same group of authors investigated the suitability of ^{64}Cu-labeled liposomes for imaging somatostatin receptor expression in neuroendocrine tumor model.[67] The peptide octreotate (TATE) was covalently attached to the PEGylated liposomes with an encapsulated positron emitter ^{64}Cu. This peptide is routinely used in clinic for imaging somatostatin receptor-positive tumors by scintigraphy.[68] *In vivo* PET imaging and biodistribution studies revealed that the presence of TATE on the liposomes resulted in a significantly faster initial blood clearance in comparison to control liposomes without TATE. There was no significant difference in tumor uptake (∼5% ID/g in both cases) on using ^{64}Cu-labeled PEGylated liposomes with or without TATE, suggesting that the uptake was mainly due to passive targeting. However, ^{64}Cu-loaded PEGylated liposomes with TATE showed significantly higher tumor-to-muscle (T/M) ratio (12.7 ± 1.0) than the control-liposomes without TATE (8.9 ± 0.9). The tumor accumulation and T/M ratio achieved in this study suggest that lioposomal systems might be used as carriers of radionuclides for therapeutic use and also for delivery of chemotherapeutic drugs.

Tumor associated macrophages (TAMs) have been shown to play a major role in the growth and spread of several types of cancer.[69,70] Locke et al. reported PET imaging of TAMs in a mouse model of pulmonary adenocarcinoma, using mannose coated liposomes radiolabeled with ^{64}Cu.[71] *In vivo* PET imaging and biodistribution studies revealed that radiolabeled mannosylated liposome accumulated in TAMs and exhibited little accumulation in remote lung areas at 6 h post injection. Further, it was verified by confocal microscopy that the PET signal was due to liposome internalization by TAMs. Urakami et al. developed a methodology for one-step labeling of liposomes with ^{18}F.[72] Solid-phase transition method was utilized, and high labeling efficiency and visualization of liposomal trafficking in mice by real-time analysis were obtained by PET. The same group reported the development of an efficient method for preparation of ^{18}F-labeled liposome-encapsulated hemoglobin.[73] Using the radiolabeled liposome, the oxygen transfer even in an ischemic brain could be monitored by dynamic PET. In another study, radiolabeling of PEGylated liposomes with [^{18}F]fluorodipalmitin ([^{18}F]FDP) was reported by Marik et al.[74] Radiolabeled diglyceride was synthesized by the incorporation of ^{18}F into the lipid molecule by nucleophilic substitution of *p*-toluenesulfonyl moiety. While free [^{18}F]FDP was rapidly taken by the liver, spleen, and lungs, liposome incorporated [^{18}F]FDP was observed to circulate in blood vessels for nearly 90 min.

Adopting the previously reported procedures,[63,74] ^{18}F and ^{64}Cu-labeled liposomes were prepared by Paoli et al.[75] The liposomes were preconjugated with suitable fluorophores (calcein or AF-750), for dual-modality PET/optical imaging. A model hydrophilic drug was encapsulated in the liposomal system and administered in mice bearing bilateral Met-1 tumors. Using *in vivo* PET imaging and *ex vivo* fluorescent imaging of tumors, the authors could demonstrate that the accumulation of the drug was increased by up to 177-fold by liposomal encapsulation. Recently, Oku et al. reported the radiolabeling of liposomes [modified with PEG or Ala-Pro-Arg-Pro-Gly (APRPG) peptide] with 1-[^{18}F]fluoro-3,6-dioxatetracosane, which enabled imaging of gliomas by PET with higher contrast than that obtained with [^{18}F]fluorodeoxyglucose ([^{18}F]FDG).[76] The liposomes did not accumulate in the normal surrounding brain tissue due to blood−brain barrier protection, and using this approach, even a very small sized (∼1 mm) brain tumor could be specifically imaged with the radiolabeled liposome (Figure 1). Mitchell et al. developed a series of liposomal systems with oligoethylene glycol spacers of differing lengths between the 1,4,7,10-tetraazacyclododecane-1,4,7,10-tetraacetic acid (DOTA) chelator and the lipid headgroup.[77] A suitable fluorophore, *N*-(fluorescein-5-thiocarbamoyl)-1,2-dihexa-decanoyl-*sn*-glycero-3-phosphoethanolamine triethylammonium salt, was attached to the liposome, which could also be chelated to Gd^{3+} (for MRI), $^{111}In^{3+}$ (for

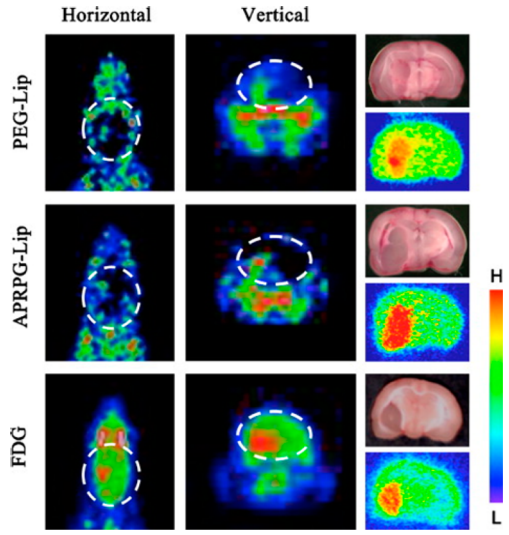

Figure 1. PET image-guided tumor targeting using liposome based carrier. PET imaging of brain tumor using PEG-modified liposomes (top panel) and APRPG-modified liposomes (middle panel), labeled with 1-[^{18}F]fluoro-3,6-dioxatetracosane. The other regions of the brain showed a low background. On the contrary, [^{18}F]FDG imaged the whole brain, although the accumulation was higher in the tumor region (bottom panel). Autoradiograms shown in the right panel confirmed the region of tumor. Adapted with permission from ref 76. Copyright 2011 Elsevier.

dx.doi.org/10.1021/mp500173s | *Mol. Pharmaceutics* 2014, 11, 3777−3797

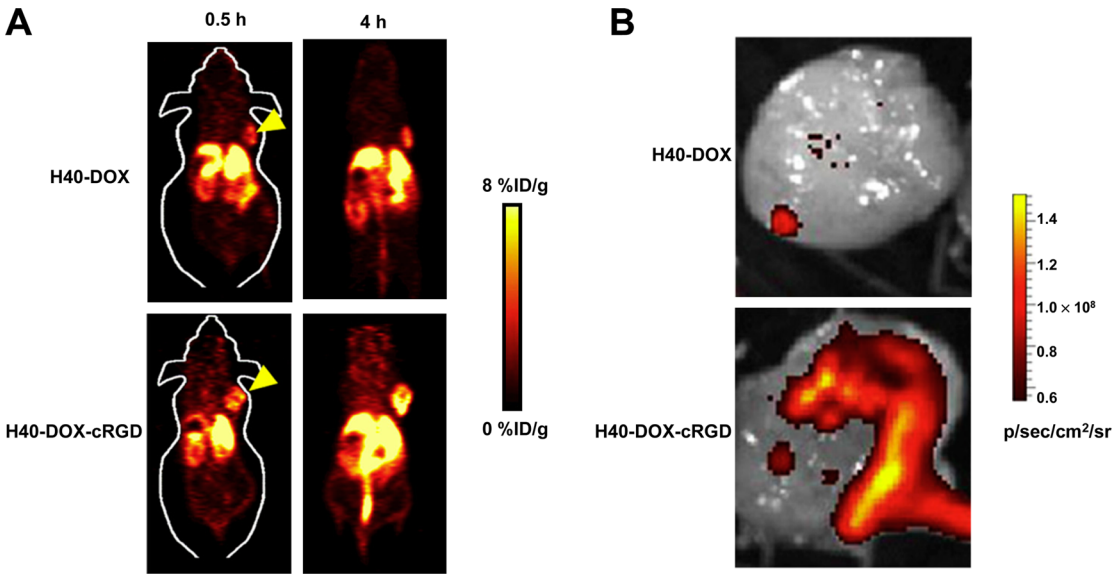

Figure 2. PET image-guided tumor targeting using micelle based carrier. (A) PET imaging of U87 tumor bearing mice at different time points post injection of ^{64}Cu-labeled unimolecular micelle loaded with DOX (H40-cRGD-^{64}Cu) and ^{64}Cu-labeled unimolecular micelle conjugated with cRGD and loaded with DOX (H40-DOX-cRGD-^{64}Cu). Adapted with permission from ref 86. Copyright 2012 Elsevier. (B) *Ex vivo* fluorescence imaging of U87MG tumor, with the excitation and emission set for detecting DOX fluorescence, harvested from mice injected with H40-DOX-^{64}Cu or H40-DOX-cRGD-^{64}Cu. Adapted with permission from ref 86. Copyright 2012 Elsevier.

SPECT), or $^{64}Cu^{2+}$ (for PET) and used for multimodal imaging. The effective radiolabeling and noninvasive imaging strategies developed thus far might aid further research on PET image-guided drug delivery using liposomal carriers in the near future.

Micelle-Based Delivery Approach. A micelle is an aggregate of surfactant molecules dispersed in a liquid colloid. Miceller structures are important carriers for drug delivery because they can form relatively small and uniform size structures, be prepared from a variety of amphiphilic materials, increase solubility of hydrophobic molecules, and incorporate multiple functionalities into a single structure.[78−80] When tagged with suitable contrast agents, these systems can also be used for molecular imaging as well as image-guided drug delivery. Among the various miceller structures, the polymeric micelles are the most extensively used for drug delivery applications.[80] The polymeric micelles generally consist of a unique core−shell structure. The inner core is the hydrophobic part of the block copolymer, which encapsulates the water-insoluble drug. The outer shell or corona of the hydrophilic block of the copolymer is often composed of PEG, and it protects the drug from the aqueous environment and also imparts particle stability and excellent dispersibility in an aqueous solution. Owing to these characteristics, polymeric micelles have several advantages as drug carriers such as enhancing the aqueous solubility of hydrophobic drugs, prolonging the circulation time of the drug in the blood, improving the *in vivo* stability of the drug, providing both passive and active tumor targeting abilities, and reducing nonspecific uptake by the reticuloendothelial system.[80]

In vivo tumor targeting and drug delivery properties of polydiacetylene (PDA) micelles (diameter ∼10 nm) were investigated by Mackiewicz et al. in a breast cancer model.[81] Such small sized micelles can better diffuse through blood vessel walls and reach deeper tumor tissues due to the EPR effect. The authors synthesized different micelles with coatings consisting of either nitrilotriacetic acids (NTA) or PEG chains of variable lengths and tested for their ability to passively target tumor. Among them, 2 kDa PEG-coated micelle (PDA-PEG2000) was identified as the most promising carrier in terms of longer blood residence time, higher tumor uptake, and better imaging contrast. Fluorescence diffuse optical tomographic imaging indicated a tumor uptake of ∼3% of the injected dose of PDA-PEG2000. The diffusion of PDA-PEG2000 micelles inside the tumor was further evidenced and quantified by PET imaging using ^{18}F-FDG colocalization. Drug delivery application of the cargo was also assessed using micelles loaded with paclitaxel, a hydrophobic anticancer drug, which showed good *in vitro* cytotoxicity and *in vivo* tumor growth inhibition. Thus, the potential of PDA-micelles for drug delivery could be successfully demonstrated in this study. In another study, Cho et al. reported a novel drug delivery strategy using poly(ethylene glycol)-*block*-poly(ε-caprolactone) (PEG-*b*-PCL) micelles.[82] Three different drugs, namely, paclitaxel (cytotoxic agent), cyclopamine (hedgehog inhibitor), and gossypol (Bcl-2 inhibitor), were loaded on PEG-*b*-PCL micelles and evaluated in xenograft models of ovarian cancer. Multi-drug-loaded PEG-*b*-PCL micelles were nanoscopic, fairly stable in aqueous solution, and capable of simultaneous as well as sustained release of each of the three drugs *in vitro*. *In vivo* studies based on bioluminescence imaging and 3′-deoxy-3′-^{18}F-fluorothymidine (^{18}F-FLT) PET imaging revealed that multi-drug-loaded PEG-*b*-PCL micelles had significantly less tumor burden than use of paclitaxel alone. Also, ^{18}F-FLT-PET images clearly showed that multi-drug-loaded PEG-*b*-PCL micelles significantly reduced tumor volumes over paclitaxel and vehicle controls and could thus prolong the overall survival. Thus, the authors could establish that the strategy of concurrent delivery of drug combinations of cytotoxic agents and molecular targeted agents using a micellar-based drug delivery vehicle is effective for the treatment of ovarian cancer.

Recently, Benezra et al. evaluated the potential of ^{18}F-labeled dasatinib derivative (SKI249380, a new-generation Src and platelet-derived growth factor receptor (PDGFR) inhibitor[83])

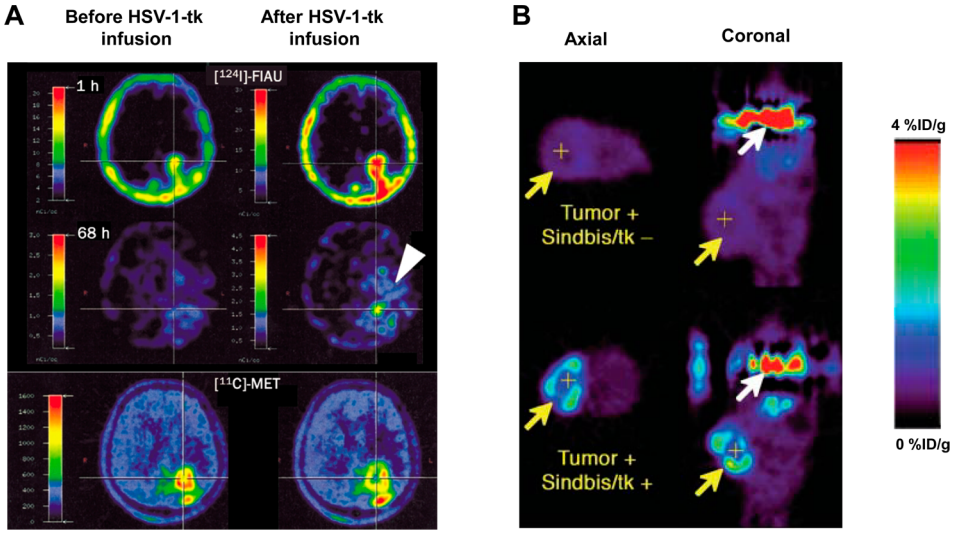

Figure 3. PET image-guided tumor targeting using enzyme/prodrug approach. (A) PET imaging using ^{18}F-FIAU to identify the location, magnitude, and extent of vector-mediated gene expression in gene therapy for recurrent glioblastoma. Treatment responses were recorded by PET imaging with ^{11}C-MET. The region of specific ^{124}I-FIAU retention within the tumor after HSV-1-tk-transduction (white arrow) showed the signs of necrosis (cross hairs, right column and reduced methionine uptake [MET]) after ganciclovir treatment. Adapted with permission from ref 98. Copyright 2001 Elsevier. (B) PET imaging of HSV-1-tk activity in tumors after Sindbis/tk infection. Tumor-bearing mice either received no vector treatment (Tumor +, Sindbis/tk −) or received 3 Sindbis/tk treatments via intraperitoneal injection far away from sites of tumor inoculation (Tumor +, Sindbis/tk +). HSV-1-tk activity was determined after intravenous administration of ^{18}F-FEAU as tracer. Tumors on the right shoulder of SCID mice are indicated by yellow arrows, and white arrows indicate activity in urinary bladder. Adapated with permission from ref 102. Copyright 2006 Society of Nuclear Medicine and Molecular Imaging.

loaded on micellar and liposomal carriers for drug delivery and uptake in xenograft models of high-grade glioma.[84] *In vivo* PET imaging studies demonstrated a significantly higher tumor uptake for ^{18}F-SKI249380-loaded micellar formulations (4.9% ID/g) compared to control group (1.6% ID/g). Saturation studies using excess cold dasatinib showed marked reduction of tumor uptake values to levels in normal brain (1.5% ID/g), consistent with *in vivo* binding specificity. The improved drug solubility, delivery, and kinetic behavior conferred by the use of these micellar ^{18}F-SKI249380 preparations might find utility in treatment of various types of gliomas.

Despite the excellent attributes of the polymeric micelles as carriers for drug delivery, such systems suffer from insufficient *in vivo* stability which is affected by the surrounding environment, especially the concentration of the amphiphilic block copolymers.[85] Upon dilution in the bloodstream, multimolecular polymeric micelles disassemble, leading to a burst release of drug and loss of tumor-targeting abilities.[85] These limitations could be circumvented with the use of suitably engineered unimolecular micelles possessing excellent *in vitro* and *in vivo* stability.[86,87] The synthesis of a multifunctional unimolecular micelle made of a hyperbranched amphiphilic block copolymer, Boltorn H40-poly(L-glutamate-hydrazone-doxorubicin)-*b*-poly(ethylene glycol), for PET image-guided drug delivery was reported by Xiao et al.[86] The copolymer was conjugated with cyclo(Arg-Gly-Asp-D-Phe-Cys) peptides (cRGD) for integrin $\alpha_v\beta_3$ targeting and macrocyclic chelators (1,4,7-triazacyclononane-*N*,*N*′,*N*″-triacetic acid [NOTA]) for ^{64}Cu-labeling and PET imaging. The anticancer drug doxorubicin (DOX) was covalently conjugated onto the hydrophobic segments of the amphiphilic block copolymer arms via a pH-labile hydrazone linkage to enable pH-controlled drug release. *In vivo* PET imaging and biodistribution studies in U87MG tumor-bearing mice showed higher tumor uptake for cRGD-conjugated unimolecular micelles (~7% ID/g) than nontargeted micelles (~2.5% ID/g) (Figure 2). Additionally, cRGD-conjugated unimolecular micelles exhibited a much higher cellular uptake in U87MG human glioblastoma cells than nontargeted unimolecular micelles due to integrin $\alpha_v\beta_3$ mediated endocytosis, thereby leading to a significantly higher cytotoxicity when the micellar systems were conjugated with DOX. The same group of authors reported the synthesis of another unimolecular micelle formed by dendritic amphiphilic block copolymers poly(amidoamine)-poly(L-lactide)-*b*-poly-(ethylene glycol) conjugated with an anti-CD105 monoclonal antibody (TRC105) and NOTA for PET image-guided drug delivery.[87] DOX was loaded into the hydrophobic core of the unimolecular micelles. As observed in the previous study, ^{64}Cu-labeled targeted micelles exhibited a much higher level of tumor accumulation than ^{64}Cu-labeled nontargeted micelles, measured by serial noninvasive PET imaging and confirmed by biodistribution studies in murine breast tumor-bearing mice. Thus, these multifunctional unimolecular micelles possessing passive and active tumor-targeting abilities, pH-controlled drug release, and PET imaging capabilities are potentially important drug delivery vehicles for image-guided therapy.

Enzyme/Prodrug-Based Delivery Approach. Enzyme/prodrug therapy is one of the most promising strategies where systemic toxicity can be minimized while maintaining the therapeutic efficacy.[88−90] In this process, a drug-activating enzyme is targeted or expressed in cancer cells, following which a nontoxic prodrug is administered systemically.[91,92] The enzyme converts the prodrug to an active anticancer drug, achieving high concentrations in the tumor and sparing the normal tissues. However, there are certain requirements for this strategy to work in clinical context. The enzyme should be non-human or expressed at very low concentrations in the normal tissue and should have high enzymatic activity. The prodrug should be a good substrate for the enzyme but should not be activated in nontumor tissues. While the prodrug should be

dx.doi.org/10.1021/mp500173s | *Mol. Pharmaceutics* 2014, 11, 3777−3797

nontoxic, the activated drug should be highly toxic and diffusible to be taken up by the adjacent cells for a "bystander cell kill effect". Ideally, the activated drug should not leak out into the systemic circulation. Currently, there are three major categories of enzyme/prodrug strategies: (a) delivery of genes that encode prodrug-activating enzymes into tumor tissue (gene encoding prodrug activating enzyme therapy, GDEPT, and virus-directed enzyme prodrug therapy, VDEPT), (b) targeted delivery of active enzymes in tumor tissue where the therapeutic enzyme is conjugated with an antibody, small molecular ligand, or peptide that binds to antigens preferentially expressed on the surface of tumor cells or in the tumor vasculature or interstitium (targeting group-directed enzyme/prodrug therapy, TDEPT), and (c) vasculature permeability-dependent enzyme/prodrug therapy (VPDEPT) in which the intratumoral delivery of the enzyme is realized through the higher permeability of tumor vasculature.[91−94] PET image-guided enzyme/prodrug strategies have been extensively reviewed and hence will be discussed briefly in the following text.[89,94−96]

Most of the studies in PET guided enzyme/prodrug based cancer therapy are based on the GDEPT approach. Bankiewicz et al. developed a strategy which combined gene therapy with aromatic L-amino acid decarboxylase (AADC) gene and a prodrug, dopamine.[97] Using this approach, the authors could synthesize and regulate the neurotransmitters involved in Parkinson's disease. *In vivo* PET imaging using AADC tracer, 6-[^{18}F]fluoro-L-*m*-tyrosine (FMT) could measure the gene expression and thus establish the potential of enzyme/prodrug approach in delivery of therapeutic agents to the central nervous system. Also, the extent of gene expression could be effectively used to predict the therapeutic response. This approach could be further validated in another study where PET imaging with ^{124}I-labeled 2′-fluoro-2′-deoxy-1b-D-arabino-furanosyl-5-iodo-uracil (^{124}I-FIAU), a specific marker substrate for expression of the herpes simplex virus type-1 thymidine kinase (HSV-1-tk) gene, was used to identify the location, magnitude, and extent of vector-mediated gene expression in a phase I/II clinical trial of gene therapy for recurrent glioblastoma.[98] In this study, dynamic ^{124}I-FIAU-PET scans were done before gene transduction to assess the basal state of FIAU-accumulation and washout of the tumor, and also after vector application to investigate whether specific FIAU-accumulation did occur (Figure 3A). Ganciclovir treatment (5 mg per kg twice a day over 14 days) was done starting 4 days after vector infusion. Treatment responses were recorded by repeated MRI as well as PET with ^{18}F-FDG and ^{11}C-labeled methionine (^{11}C-MET). The same PET tracer (^{124}I-FIAU) was used by Hackman et al. to assess the potential of double prodrug activation gene therapy using the *Escherichia coli* cytosine deaminase (CD)-HSV-1-tk fusion gene (CD/TK) for treatment of different tumors.[99] PET imaging was used for monitoring expression of the CD/TK fusion gene, and the different levels of CD/TK expression in tumor models could be imaged quantitatively. The results of these studies could be utilized to develop standardized gene therapy protocols adopting enzyme/prodrug strategy for human subjects.

The synthesis of half-mustard prodrug, 4-[(2-chloroethyl)(2-ethyl) amino]-phenoxycarbonyl-L-glutamic acid, by reductive alkylation of 4-[(2-chloroethyl)amino]-phenoxycarbonyl-L-glutamic acid was reported by Malik et al.[100] The prodrug was radiolabeled with ^{11}C, and its potential for imaging antibody- and gene-directed enzyme prodrug therapy with PET could be established. The use of another prodrug, 1-(2-deoxy-2-fluoro-β-D-arabinofuranosyl)uracil (FAU), for treatment of tumors with high thymidylate synthase catalytic activity was reported by Eiseman et al.[101] This prodrug was activated by thymidylate synthase enzyme. PET imaging using ^{18}F-FAU was used to visualize tumors that have high thymidylate synthase catalytic activity. However, the authors did not observe high localization of ^{18}F-FAU in tumors compared with background, which might limit further utilization of this PET probe in clinical context. In another study, selective tumor targeting and quantitative *in vivo* monitoring using PET of a commonly applied GDEPT, based on HSV-1-tk and ganciclovir (GCV), was reported by Tseng et al.[102] Sindbis virus was used to deliver the HSV-1-tk suicide gene to tumor cells for subsequent GCV activation and tumor killing. PET imaging using ^{18}F-labeled fluoro-ethyl-arabinosyluridine (^{18}F-FEAU) was used to monitor the HSV-1-tk activity in tumor cells after parenteral administration of Sindbis virus (Figure 3B). High tumor uptake of ^{18}F-FEAU (∼3% ID/g) proved that the Sindbis vector efficiently targeted the HSV-1-tk enzyme gene into the infected tumor cells. Also, PET imaging could be used to monitor HSV-1-tk activities after systemic Sindbis vector treatments for determining the levels and tissue distribution of the vector and optimizing efficient prodrug activation for more accurate treatment planning and monitoring. This study was further extended by Stelter et al., where different molecular imaging strategies, such as bioluminescence, fluorescence molecular tomography, and PET, were used to evaluate Sindbis virus mediated infection of tumor cells *in vitro* and *in vivo*.[103] The authors concluded that the Sindbis virus infection rates were not solely dependent on cellular laminin receptor expression and other factors such as cellular infection and viral replication might also be responsible. In another similar study, Wang et al. evaluated the efficacy of 4 different radiotracers, ^{123}I-5-iodo-29-fluoro-1-*b*-D-arabinofuranosyluracil (^{123}I-FIAU), 5-^{18}F-fluoro-29-deoxyuridine (^{18}F-FUdR), 2-^{18}F-fluoroethyl-L-tyrosine (^{18}F-FET), and ^{18}F-FDG for monitoring tumor responses using SPECT or PET during prodrug activation gene therapy with HSV-1-tk and GCV.[104] Based on tumor uptake of the radiotracers, ^{18}F-FUdR was identified as the most suitable radiotracer for assessment of responses in tumors undergoing HSV-1-tk and GCV prodrug activation gene therapy.

The enzyme β-glucuronidase (β-GUS) has recently been investigated as a target in prodrug therapy for cancer.[105−107] In order to optimize β-GUS-based prodrug therapies, a PET tracer, ^{18}F-labeled 1-*O*-(4-(2-fluoroethyl-carbamoyloxymethyl)-2-nitrophenyl)-*O*-β-D-glucopyronuronate (^{18}F-FEAnGA), was evaluated for imaging of β-GUS in tumor (C6 gliomas) and inflammation models.[106] *In vivo* PET imaging and biodistribution studies showed high uptake of the radiotracer in tumor, high target to nontarget ratio, and rapid renal clearance. In inflammation model, the uptake of the radiotracer in inflamed muscle was significantly higher than in control muscle, thereby establishing the potential of this radiotracer to detect increased activity of β-GUS. The extent of β-GUS release in small C6 glioma tumors after a single treatment of doxorubicin (DOX), carmustine (BCNU), and tumor necrosis factor α (TNF-α) with ^{18}F-FEAnGA PET was evaluated by the same group of authors.[107] PET studies confirmed that β-GUS was released *in vivo* and the distribution volume of ^{18}F-FEAnGA in C6 gliomas was increased significantly. These results were further confirmed by histochemical analysis and flow cytometry. The results obtained in this study demonstrate the potential of

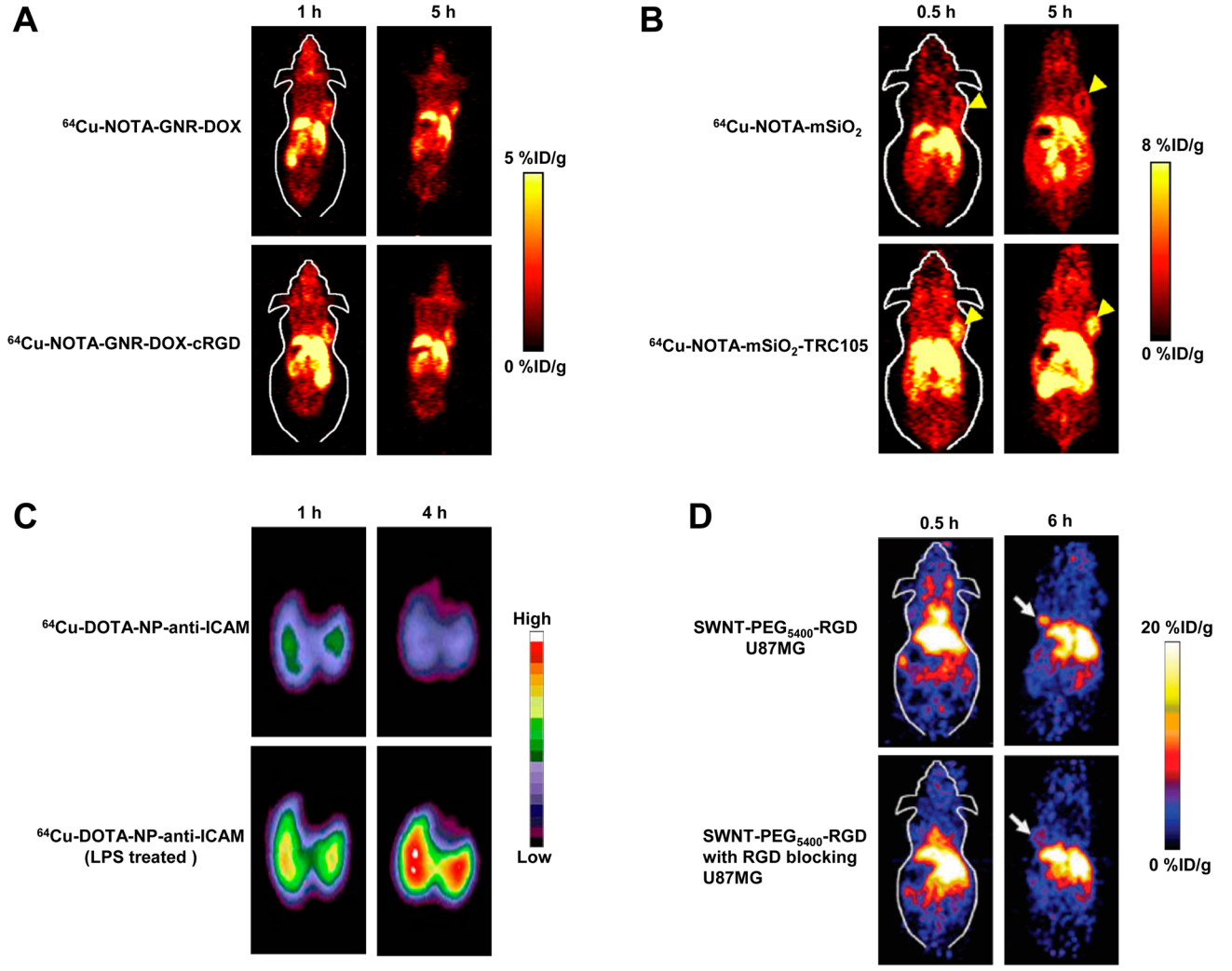

Figure 4. PET image-guided tumor targeting using nanoparticle based carrier. (A) Targeting of integrin $\alpha_v\beta_3$ expression in U87MG tumor bearing mice by gold nanorods (GNR) conjugated with cRGD. PET images at different time points post injection of ^{64}Cu-labeled gold nanorods conjugated with DOX (^{64}Cu-NOTA-GNR-DOX) and ^{64}Cu-labeled gold nanorods conjugated with DOX and cRGD (^{64}Cu-NOTA-GNR-DOX-cRGD). Arrowheads indicate the tumors. Adapted with permission from ref 132. Copyright 2012 Ivyspring International Publisher. (B) Targeting of CD105 expression in 4T1 tumor-bearing mice by TRC105-conjugated mesoporous silica nanoparticles. PET images at different time points post injection of ^{64}Cu-labeled mesoporous silica (^{64}Cu-NOTA-mSiO$_2$) and ^{64}Cu-labeled mesoporous silica conjugated with TRC105 (^{64}Cu-NOTA-mSiO$_2$-TRC105). Tumors were indicated by yellow arrowheads. Adapted with permission from ref 142. Copyright 2013 American Chemical Society. (C) Targeting of lung endothelium in C57BL/6 mice by polymeric nanoparticles conjugated with anti-ICAM antibody. Micro-PET images of mice at different time points post injection of ^{64}Cu-labeled nanoparticle conjugated with anti-ICAM antibody (^{64}Cu-DOTA-NP-anti-ICAM) and ^{64}Cu-labeled nanoparticle conjugated with anti-ICAM antibody after pretreating the mice with lipopolysaccharides (^{64}Cu-DOTA-NP-anti-ICAM LPS treated). Adapted with permission from ref 153. Copyright 2008 Society of Nuclear Medicine and Molecular Imaging. (D) Targeting of integrin $\alpha_v\beta_3$-expression in U87MG tumor bearing mice by cRGD-functionalized single walled carbon nanotubes (SWNTs). PET images showing high tumor uptake of SWNT−PEG$_{5400}$−RGD observed in the U87MG tumor (first row) and control experiment showing blocking of SWNT−PEG$_{5400}$−RGD tumor uptake by coinjection of free cRGD (second row). The arrows point to the tumors. Adapted with permission from ref 165. Copyright 2007 Nature Publishing Group.

a two-step chemotherapy−prodrug approach, in which tumors are treated with a single dose of a cytostatic drug before prodrug treatment. Recently, Moon et al. reported the synthesis of ^{18}F labeled 1-(3-furyl)-4-hydroxy-5-fluoro-1-pentanone (^{18}F-F-4-IM), which can be metabolized by the CYP4B1 enzyme and used for PET imaging of tumors and monitoring enzyme-activating anticancer prodrugs.[108] Biodistribution studies in normal rats showed that the uptake of ^{18}F-F-4-IM was high in the lung, where CYP4B1 gene is preferentially expressed. The results were further confirmed by *in vitro* cell assays, and the potential of ^{18}F-F-4-IM for imaging of CYP4B1-transfected tumor cells and monitoring CYP4B1 enzyme/prodrug interactions could be demonstrated. It is envisaged that further development of PET guided enzyme/prodrug protocols would significantly facilitate their clinical translation with high safety and reliability.

Nanoparticle-Based Delivery Approach. In the past two decades, the applications of nanotechnology in cancer diagnostics and therapy have attracted widespread interest and a variety of functional nanoparticles have been developed and evaluated for drug delivery, diagnostic sensors, imaging agents, and labeling probes.[109−120] Nanoparticles used for this purpose vary with a size from 1 nm to few hundred nanometers and surface charge varying from negative to positive and even

dx.doi.org/10.1021/mp500173s | *Mol. Pharmaceutics* 2014, 11, 3777−3797

neutral. Particularly as drug delivery vehicles and molecular imaging tools, targeted nanoparticle based systems hold significant promise by virtue of their controllable size, high surface area to volume ratio, and customized internal and external chemistries. The major advantages of using the engineered nanoparticle based systems for such applications include (a) the ease of particle functionalization for conjugation with suitable targeting vectors such as peptides or antibodies, (b) the ability to deliver a higher concentration of contrast agent for every targeted binding event to achieve higher detection sensitivity which might permit diagnosis of the disease in its very early stage, and (c) improved treatment effects when used as drug carriers by protecting entrapped drugs from degradation, enhancing tumor uptake through the enhanced permeability and retention effect as well as receptor-mediated endocytosis and thereby achieving increased exposure of the tumor to therapeutic drugs. A variety of drug delivery systems based on metallic nanoparticles, oxide nanoparticles, polymeric nanoparticles, carbon nanostructures, biodegradable nanoparticles, etc. have been developed for molecular imaging as well as drug delivery.[121−125] For a given system, multiple factors determine the stability and fate of the delivery vehicle during storage and after administration, including size, rigidity, charge, solubility, and surface modifications of the nanoparticles. Therefore, the choice of a nanoparticle based delivery system is guided by the biodistribution, types of drugs that can be delivered using that system, and the specificity and pharmacokinetics of delivery. The different nanoparticle based systems which can be radiolabeled with suitable positron emitting radioisotopes for PET image-guided drug delivery are discussed in the following text.

Metallic Nanoparticles. Among the various metallic nanoparticles reported to date, gold nanoparticles are most widely used for biomedical applications, including drug delivery and novel diagnostic and therapeutic approaches, due to their biocompatibility, small size, ease of characterization, and rich surface chemistry.[126−129] The utilization of ^{18}F-labeled gold nanoparticles for PET imaging was first reported by Guerrero et al.,[130] in which the gold nanoparticles of ∼12 nm were synthesized by citrate reduction of $HAuCl_4$. The nanoparticles were functionalized with two different peptides, CK and CLPFFD, and ^{18}F-SFB was covalently bound to the nanoparticle conjugate. After intravenous administration of the radiolabeled nanoparticles in normal rats, *in vivo* PET imaging showed highest uptake of the radioactivity in the bladder. The lungs, liver, and spleen were the organs with the next highest levels of radioactivity, followed by the intestine, kidneys, and blood. The pancreas and brain, however, accumulated very low concentrations of radiolabeled nanoparticles. Clearance of the nanoparticles from the biological system took place by both renal and biliary excretions.

Gold nanorods with suitable aspect ratios can absorb and strongly scatter light in the near-infrared region, which can be used for enhanced optical imaging and photothermal cancer therapy.[131] The development of a multifunctional gold nanorod-based nanoplatform for targeted anticancer drug delivery and PET imaging of tumors was reported by Xiao et al.[132] The bare gold nanorods had a length and diameter of approximately 45 and 10 nm, respectively. An anticancer drug (DOX) and tumor targeting agent (cRGD) were conjugated to the PEGylated gold nanorods. Also, NOTA was attached onto the distal ends of the PEG arms for complexation with ^{64}Cu. Based on flow cytometry analysis, cRGD-conjugated gold nanorods exhibited a higher cellular uptake and cytotoxicity than nontargeted ones *in vitro*. However, *in vivo* PET imaging and biodistribution studies showed that targeted and nontargeted gold nanorods had similar distribution pattern especially in the tumor (Figure 4A). Despite this limitation, this initial attempt provided a suitable nanoplatform for possible integration of multifunctionality including molecular targeting, chemotherapy, and photothermal therapy, as well as multimodality imaging, which can potentially lead to improved therapeutic efficacy and cancer monitoring. To achieve a similar goal, Xie et al. reported the preparation of ^{64}Cu-labeled gold nanoshells conjugated with cRGD and studied the *in vivo* biodistribution and tumor specificity using PET.[133] The nanoshell used in this study was composed of a silica core (∼120 nm in diameter) and a gold shell (8−10 nm) to absorb light at near-infrared wavelengths. *In vivo* PET imaging suggested that tumor targeting was improved by conjugation of gold nanoshells to cRGD, which was advantageous over the previous study by Xiao et al.[132] Both targeted and nontargeted gold nanoshells were cleared from the circulation by the liver and spleen. In the subablative thermal therapy study, enhanced biological effectiveness of targeted gold nanoshell was shown by the higher degree of tumor necrosis compared with nontargeted nanoshell. The promising results obtained from this study might lead to advancement of gold nanoshells as theranostic platforms for effective cancer diagnosis and therapy.

Oxide Nanoparticles. Another category of promising nanoplatforms which has drawn substantial interest recently is the oxide nanoparticles (such as mesoporous silica and iron oxide nanoparticles) due to their nontoxic nature, easily modifiable surface, and good biocompatibility.[134,135] The utilization of core−shell silica nanoparticles as targeted PET/optical multimodal imaging probes was reported by Benezra et al.[136] Near-infrared fluorescent, Cy5 dye-encapsulated, core−shell silica-based nanoparticles were prepared and coated with PEG as per the method reported by Burns et al.[137] The nanoparticle was conjugated with cRGD and radiolabeled with ^{124}I through a tyrosine linker. *In vitro* cell binding assays demonstrated the specificity of the nanoplatform toward intregrin $\alpha_v\beta_3$ expression. *In vivo* PET/optical imaging and biodistribution studies showed a tumor uptake of ∼1.5% ID/g at 4 h post injection, with high tumor to background ratio and rapid renal clearance. Owing to their favorable characteristics, such as bulk renal clearance, favorable targeting kinetics, lack of acute toxicity, superior photophysical features, and multimodal (PET/optical) imaging capabilities, such nanoparticles have received the United States Food and Drug Administration (US FDA)-investigational new drug approval for a first-in-human clinical trial.[138]

The synthesis of ultrasmall, monodisperse silica nanoconjugates for targeted dual-modal imaging of lymph nodes with metastatic tumors was reported by Tang et al.[139] The nanoparticles were functionalized with an aptamer derivative having high binding affinity for nucleolin, a protein that is overexpressed in the cytoplasm and on the plasma membrane of several cancer cells. Also, a near-infrared (NIR) dye and DOTA were conjugated on the surface of the functionalized nanoparticle. The aptamer functionalized silica nanoconjugate was radiolabeled with ^{64}Cu, and *in vivo* PET/optical imaging studies showed markedly enhanced uptake of the radiolabeled agent in lymph nodes with metastatic tumors in a murine breast tumor model. In a similar study, Kim et al. reported the development of a core−shell silica nanoprobe for multimodal

(PET/optical/MRI) imaging of the sentinel lymph node.[140] Magnetic silica nanoparticles with cobalt ferrite core and silica shell were synthesized which encapsulated NIR dye on the silica shell. The surface of the nanoparticle was modified with amino group and PEG for conjugation with NOTA, which was used for chelating ^{68}Ga. The triple modality nanoprobe could be successfully utilized to visualize the sentinel lymph node in mice. Thus, these multimodal silica nanostructures hold great potential for improving the accuracy of clinical tumor staging by serving as probes for efficient noninvasive targeted imaging of metastatic lymph nodes. Different chemotherapeutic drugs can also be attached on the surface of the functionalized nanoconjugates for prevention of metastases.

In an interesting study, Di Pascua et al. utilized commercially available mesoporous silica nanoparticles as a carrier material for the therapeutic radioisotope ^{166}Ho ($t_{1/2}$ = 26.8 h, $E_{\beta max}$ = 1.84 MeV).[141] A lipophilic acetylacetonate complex of ^{165}Ho was incorporated in mesoporous silica nanoparticles (80−100 nm in diameter), which were subsequently irradiated in a neutron flux to produce particles containing ^{166}Ho by (n,γ) reaction. These radioactive nanoparticles were utilized to deliver effective therapeutic doses for treating ovarian cancer metastases after intraperitoneal delivery in SKOV-3 ovarian tumor-bearing mice. *In vivo* SPECT imaging demonstrated that most of the ^{166}Ho-containing mesoporous silica nanoparticles administered to ovarian tumor-bearing mice were retained in the peritoneal cavity and selectively accumulated in the tumors (33% ID/g after 24 h). Radiotherapeutic efficacy was monitored using PET/CT using ^{18}F-FDG which showed a decrease in tumor volume, which correlated with a marked increase in survival after treatment with ∼4 MBq of the radioactive nanoparticles. Though the authors could not explain the reason for the high uptake of mesoporous silica nanoparticles in ovarian tumor, this strategy might find utility in incorporation with other therapeutic radionuclides in nanostructured materials for treatment of various types of cancer. In another approach, Chen et al. reported the development of biocompatible functionalized mesoporous silica nanoparticles for actively targeted PET imaging and chemotherapeutic drug delivery.[142] Mesoporous silica nanoparticles were surface functionalized with thiol groups, PEGylated, conjugated with NOTA chelator and TRC105 antibody (specific for CD105/endoglin), and radiolabeled with ^{64}Cu. *In vivo* PET imaging and biodistribution studies in 4T1 breast tumor bearing mice showed high tumor uptake (∼6% ID/g) at 5 h post injection (Figure 4B). The tumor uptake of radiolabeled nanoparticles not conjugated with TRC105 was much lower than the tumor uptake observed with TRC105 conjugated nanoparticles, indicating that active targeting was responsible for the enhanced tumor uptake. The authors also demonstrated the feasibility of enhanced tumor targeted drug delivery *in vivo* using TRC105 conjugated mesoporous silica loaded with an anticancer drug, DOX. The encouraging results obtained in this study hold promise for future image-guided drug delivery and targeted cancer therapy using this class of nanomaterials.

Recently, iron oxide nanoparticles have been actively investigated as nanoplatforms for multimodal molecular imaging.[143−145] The conventional drug loading approach by covalent linkage on such nanoplatforms is inefficient and suboptimal for drug release.[146] In order to circumvent this limitation, Xie et al. synthesized iron oxide nanoparticles, modified their surface using dopamine, and encapsulated them into human serum albumin matrices, which are clinically utilized as drug carriers.[147] The human serum albumin coated iron oxide nanoparticles were dually labeled with ^{64}Cu-DOTA and Cy5.5 dye, and tested in a subcutaneous U87MG xenograft mouse model. *In vivo* PET/optical/MR imaging showed a high tumor uptake (∼5% ID/g at 4 h post injection) with high tumor to background ratio. An inhomogeneous particle distribution pattern was observed with MRI, but PET and optical imaging showed homogeneous intensities at the tumor area. The human serum albumin coated nanoparticles manifested a prolonged circulation half-life. Adopting this strategy, small drug molecules can be coloaded with iron oxide nanoparticles into human serum albumin to yield theranostic agents. Recently, Chen et al. reported a chelator free approach for preparation of radioarsenic labeled iron oxide nanoparticles.[148] The radiolabeled nanoparticle was used as PET/MRI agent for dual-modality imaging *in vivo* and lymph node mapping. This strategy can be extended for radiolabeling iron oxide nanoparticles with ^{77}As for radiotherapeutic applications.[149] In another study, Yang et al. reported the synthesis of cRGD-functionalized, DOX-conjugated, and ^{64}Cu-labeled iron oxide nanoparticles for targeted anticancer drug delivery and PET/MR imaging.[150] *In vivo* PET imaging and biodistribution studies in U87 tumor bearing mice showed that cRGD-conjugated iron oxide nanocarriers showed a much higher level of tumor accumulation (∼5% ID/g) than cRGD-free ones (<2% ID/g). Also, cRGD-conjugated nanocarriers induced a significant amount of cytotoxicity in the U87MG tumor cells, suggesting that DOX was released from the iron oxide nanocarrier and entered the cell nucleus. Thus, the potential of iron oxide nanoparticles for combined tumor-targeting drug delivery as well as multimodal imaging could be amply demonstrated.

Polymeric Nanoparticles. In recent times, there has been widespread interest in the use of biocompatible and biodegradable polymer nanoparticles for drug delivery.[151] Bartlett et al. reported the synthesis of nanoparticles using cyclodextrin-containing polycations and siRNA sequence targeting luciferase mRNA.[152] A bifunctional chelator, DOTA, was conjugated to the 5′ end of siRNA and used for labeling with ^{64}Cu. A dual-modality (PET/optical) imaging approach was used to investigate the biodistribution and functional activity of siRNA delivered by the nanoparticles. *In vivo* PET/CT imaging in mice bearing luciferase-expressing Neuro2A tumors was used to analyze the biodistribution and tumor localization of the siRNA nanoparticles. Also, bioluminescent imaging was used before and after PET imaging to enable correlation of functional efficacy with biodistribution data. It was observed that both nontargeted and transferrin-targeted siRNA nanoparticles exhibited similar biodistribution and tumor localization. However, transferrin-targeted siRNA nanoparticles could reduce tumor luciferase activity by ∼50% relative to nontargeted siRNA nanoparticles, 1 d after injection. Compartmental modeling was used to demonstrate that the primary advantage of targeted nanoparticles was associated with processes involved in cellular uptake in tumor cells rather than overall tumor localization. The authors inferred that optimization of internalization might be the key factor for effective targeted therapy using this class of nanoparticles.

The utilization of PET to quantify the uptake of intercellular adhesion molecule 1 (ICAM-1) targeted, ^{64}Cu-labeled polymeric nanoparticles by the pulmonary endothelium was reported by Rossin et al.[153] *In vivo* PET imaging and

biodistribution studies showed a 3- to 4-fold higher uptake in the lungs of mice injected with ICAM-targeted nanoparticles compared to that of the control group (Figure 4C). The lung uptake could be further enhanced by pretreating the mice with lipopolysaccharides probably due to ICAM-1 upregulation. However, a considerable release of small ^{64}Cu-radiometabolites from the nanoparticles beginning as early as 1 h after injection was observed, suggesting poor *in vivo* stability of the radiolabeled conjugate. An improved strategy where the radiolabeled nanoparticle remained stable *in vivo* was reported by Simone et al.[154] The authors developed a polymeric nanoparticle using a poly(4-vinylphenol) polymer backbone which could directly be radiolabeled with ^{124}I. The polymeric nanoparticles were coated with monoclonal antibodies targeting endothelial determinants. The radiolabeled nanoparticles were used for imaging the pulmonary vasculature and also for tracking the nanoparticle pharmacokinetics. This approach might find utility in image-guided delivery of therapeutics to the pulmonary endothelium in patients with acute and chronic respiratory diseases.

The synthesis and utilization of poly(*N*-vinylpyrrolidone)-*b*-poly(ε-caprolactone) nanoparticles (∼100 nm diameter) for drug delivery was reported by Zhu et al.[155] The nanoparticles were conjugated with a near-infrared fluorescent dye, NIR-797, for *in vivo* optical imaging. An anticancer drug, paclitaxel (PTX), was loaded in the polymeric nanoparticles with high drug loading content (>25%) and encapsulation efficiency (>85%). The antitumor effect of PTX-loaded nanoparticles was evaluated, both *in vitro* on three different cancer cell lines and *in vivo* on a hepatic H22 tumor bearing mouse model using optical imaging. The antitumor effects of the PTX-loaded nanoparticles were further visualized using ^{18}F-FDG PET scans. By combining the tumor volumes and survival rate measurements, it could be confirmed that PTX-loaded nanoparticles exhibited superior *in vivo* antitumor effect than Taxol (commercially available formulation of paclitaxel). In a similar study, Liu et al. reported the synthesis of poly(ethylene glycol)-poly(caprolactone) nanoparticles (∼70 nm diameter) and evaluated their efficacy for drug delivery.[156] As in the previous case, the polymeric nanoparticles were conjugated with NIR-797 dye for investigating the biodistribution of the drug-loaded nanoparticles using *in vivo* optical imaging. An anticancer drug, docetaxel (DOC), could be encapsulated into the polymeric nanoparticles with a high drug loading content (∼20%) and encapsulation efficiency (>80%). *In vitro* cytotoxicity test showed that DOC-loaded nanoparticles inhibited the murine hepatic carcinoma cell line H22 in a dose-dependent manner, which was similar to Taxotere, the commercialized formulation of docetaxel. However, *in vivo* tumor evaluation using optical imaging and ^{18}F-FDG PET scans demonstrated the superiority of DOC-loaded polymeric nanoparticles over Taxotere. Therefore, it could be envisaged that these highly efficient and biodegradable nanoparticles might find clinical utility in PET image-guided anticancer drug delivery in the near future.

In a pioneering study, Zhou et al. reported the synthesis of poly(lactide-*co*-glycolide) nanoparticles (∼70 nm diameter), which could be utilized as brain penetrating nanocarriers for the treatment of glioblastoma.[157] In order to illustrate the translational potential of brain-penetrating nanoparticles, the authors conducted a screen of ∼2,000 compounds that were previously approved by US FDA to inhibit patient-derived brain cancer stem cells and encapsulated the best agent (dithiazanine iodide) into the nanocarrier. The nanoparticles were radiolabeled with ^{18}F using streptavidin/biotin chemistry. The radiolabeled brain-penetrating nanocarriers were administered by convection-enhanced delivery in rats bearing brain cancer stem cell derived xenografts. *In vivo* PET imaging demonstrated accumulation of the nanoparticles in the brain. Also, a significantly increased survival in rats bearing brain cancer xenografts was observed, which demonstrated the potential of such brain-penetrating nanoparticles for targeted image-guided drug delivery for treatment of brain tumors.

With a different strategy, Chen et al. employed anionic poly(L-glutamic acid) as a carrier to covalently link with camptothecin (an anticancer drug), enabling encapsulation into supramolecular nanoparticle vectors.[158] Approximately five camptothecin molecules were conjugated to each polymer chain by ester bond formation, which could be degraded via esterase-mediated hydrolysis to allow controlled release of camptothecin under physiological conditions. The supramolecular nanoparticle was further conjugated with DOTA for ^{64}Cu labeling. The authors synthesized nanoparticles of two different sizes (37 and 104 nm), both of which were radiolabeled with ^{64}Cu and administered in mice bearing Lewis lung carcinoma xenografts. *In vivo* PET imaging and biodistribution studies revealed that the smaller sized (37 nm) nanoparticles exhibited higher tumor accumulation due to the EPR effect. The superior *in vivo* antitumor efficacy of the 37 nm supramolecular nanoparticles was further validated by tumor reduction/inhibition studies. Despite the encouraging results, the tumor uptake of the supramolecular nanoparticles was not impressive, which might be a deterrent for their use as potential drug delivery vehicles. However, the tumor uptake might be improved on conjugation with suitable targeting ligands.

Homopolymers or copolymers have long been explored as potential carriers in targeted drug delivery.[159] The synthesis and characterization of PEGylated star-shaped copolymer nanoparticles (25−70 nm size) containing core−shell morphology for *in vivo* PET imaging was reported by Fukukawa et al.[160] These copolymers possessed a hydrophilic inner shell bearing reactive functional groups, and a central hydrophobic core. DOTA was conjugated to the functional groups in the inner shell for ^{64}Cu labeling. *In vivo* PET imaging and biodistribution studies in normal rats showed that copolymers with increasing PEG shell thickness showed increased blood circulation and low accumulation in excretory organs. This preliminary study suggested the potential of such systems as for *in vivo* tumor imaging and targeted drug delivery. The synthesis of *N*-(2-hydroxypropyl)methacrylamide (HPMA) copolymers for PET imaging and image-guided chemotherapy of prostate cancer was reported by Yuan et al.[161] The HPMA copolymer was conjugated with DOTA for ^{64}Cu labeling and also with cRGD peptide for targeting $\alpha_v\beta_3$ integrin in tumor neovasculature. The tumor localization of the radiolabeled copolymer was visualized by PET in a mouse model bearing human prostate cancer xenografts. A time-dependent increase in radioactivity uptake in tumor-bearing mice injected with the HPMA-cRGD-DOTA-^{64}Cu copolymers was observed, but this phenomenon was not seen in mice injected with control HPMA-DOTA-^{64}Cu copolymers. However, the tumor uptake observed for the targeted copolymer (2.75% ID/g) at 3 h post injection was slightly higher than what was observed with the nontargeted copolymer (1.29% ID/g), suggesting that, along with active targeting, passive EPR effect also plays a partial role in tumor localization of the radiolabeled copolymer. The findings from these studies might set the stage for further optimization and

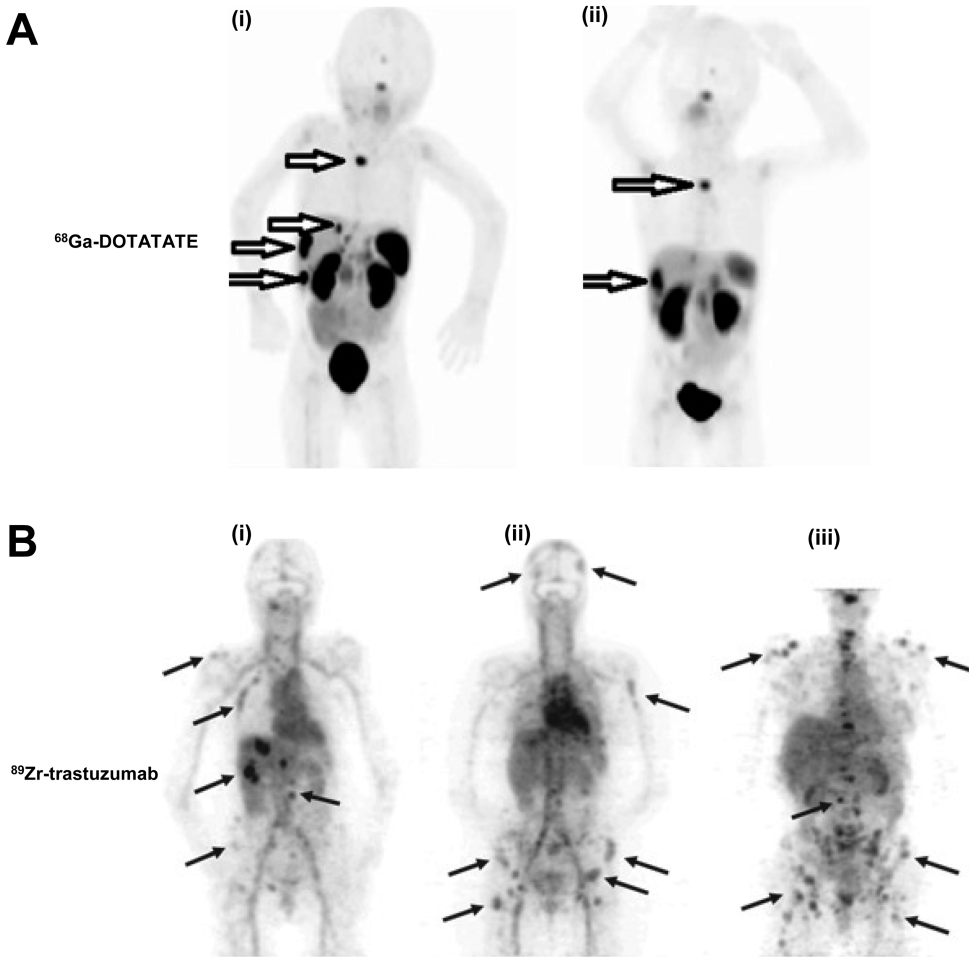

Figure 5. PET image-guided tumor targeting using conventional radiopharmaceuticals. (A) ^{68}Ga-DOTATATE PET/CT. (i) Images showing ^{68}Ga-DOTATATE avid lesions in T4 vertebral body and 3 metastases in liver (arrow). Physiologic uptake is seen in pituitary, kidneys, bladder, stomach wall, liver, and spleen. (ii) Images from repeated ^{68}Ga-DOTATATE PET/CT 1 y later after 3 administrations of ^{177}Lu-DOTATATE, showing metabolic partial response with reduction in SUV_{max} of lesion in T4 and liver and no new lesions. Adapted with permission from ref 190. Copyright 2011 Society of Nuclear Medicine and Molecular Imaging. (B) ^{89}Zr-trastuzumab PET/CT. (i) A patient with liver and bone metastases, and (ii and iii) two patients with multiple bone metastases. A number of lesions have been specifically indicated by arrows. Adapted with permission from ref 198. Copyright 2010 Nature Publishing Group.

evaluation of the copolymer constructs for image-guided drug delivery in various tumor models.

Carbon-Based Nanomaterials. Owing to their unique physical and chemical properties, the use of functionalized carbon-based nanomaterials is gaining popularity in many areas of biomedical research, including molecular imaging and drug delivery.[162] Since their discovery, the carbon nanotubes have become the most widely used carbon-based nanomaterial for biomedical applications.[162−164] PET imaging using PEGylated single walled carbon nanotubes (1−5 nm diameter, 100−300 nm length) conjugated with RGD peptides was reported by Liu et al.[165] DOTA was attached to the termini of the PEG chains and used to conjugate ^{64}Cu. *In vivo* PET imaging and biodistribution studies showed that PEG_{5400} modified single walled carbon nanotubes conjugated with cRGD exhibited a high tumor uptake of 10−15% ID/g, with high target to nontarget ratio (Figure 4D). High tumor uptake of the radiolabeled single walled carbon nanotubes was observed over long periods (>24 h). In another study, McDevitt et al. studied the biodistribution pattern of ^{86}Y labeled carbon nanotubes (∼1 nm diameter, ∼50 nm length) without PEG modification in normal mice.[166] The radiolabeled agent cleared from the blood within 3 h and distributed predominantly to the kidneys, liver, spleen, and bone. Suitable PEG modification of carbon nanotubes is of paramount importance in order to reduce reticuloendothelial system uptake and prolong blood circulation time of the single walled nanotubes for finding utility in drug delivery approaches.

Graphene is another structurally robust, yet highly flexible, nanoplatform with potential for use as a drug delivery vehicle.[162] Hong et al. reported the synthesis of covalently functionalized nanographene oxide sheets (10−50 nm), which were PEGylated and conjugated with anti-CD105 monoclonal antibody (TRC105) for imaging tumor angiogenesis.[167] The PEGylated graphene oxide was also conjugated with NOTA for ^{64}Cu labeling. *In vitro* studies using human umbilical vein endothelial cells (HUVECs, high CD105 expression) demonstrated strong and specific CD105-binding by the TRC105 conjugated nanographene. Also, *in vivo* PET imaging and biodistribution studies in 4T1 tumor bearing mice showed high tumor uptake (∼6% ID/g) within 0.5 h post injection, which remained fairly stable over time. These studies were further validated by *ex vivo* histological analyses, and vasculature specific targeting with little extravasation of TRC105

conjugated graphene oxide could be demonstrated. The same group further evaluated ^{66}Ga-labeled nanographene oxide conjugated with TRC105, and similar results were obtained.[168] This work was further improved by using ^{64}Cu-labeled reduced graphene oxide conjugated with TRC105 for *in vivo* tumor vasculature targeting.[169] Reduced graphene oxide has more desirable properties for photothermal therapy than the more hydrophilic graphene oxide used in the previous studies, due to its strong absorbance in the near-infrared range.[170] *In vivo* PET imaging revealed rapid tumor uptake (~5.5% ID/g) of ^{64}Cu-labeled nanoplatform with excellent tumor contrast. In all these studies, TRC105 conjugated nanoparticles exhibited little extravasation in the 4T1 tumor, indicating the advantages of tumor vasculature targeting using such nanoplatforms. It can be envisaged that the promising results obtained in these studies can open up new avenues for image-guided drug delivery and cancer therapy using graphene oxide based nanoplatforms.

Conventional Radiopharmaceutical-Based Delivery Approach. The drug delivery systems discussed thus far were mostly limited to chemotherapy. The concept of "theranostics" has also played a vital role in radiation-based therapies, especially, using targeted radiopharmaceuticals.[171,172] In this approach, a radiation dose is specifically administered to the cancerous lesions using peptides, proteins, or antibodies radiolabeled with suitable therapeutic radionuclides such as ^{90}Y, ^{131}I, or ^{177}Lu. The same targeting ligands can also be conveniently radiolabeled with suitable positron emitters such as ^{18}F, ^{68}Ga, ^{64}Cu, or ^{89}Zr, thereby providing exciting opportunities to guide such therapies using PET.[19,24,172−174] This approach plays a dominant role in diagnosis of the disease in its early stage, validation of the targeting strategy, and development of novel therapeutic radiopharmaceuticals. Thus, it facilitates better, faster, and cost-effective decision making, helping to eliminate failures in the targeted radiotherapy pathway and advance only with the promising candidates to receive such therapies. Despite the availability of a wide variety of PET radiopharmaceuticals, ^{18}F-FDG is still the most widely used radiotracer in cancer management, and the pivotal role of ^{18}F-FDG-PET/CT in modern nuclear medicine needs hardly to be reiterated.[175,176] Excellent review articles have appeared in recent times which have summarized the clinical diagnosis and therapeutic response evaluation using ^{18}F-FDG and other ^{18}F-based radiotracers, and hence these are not discussed here further.[176−182]

Another PET radioisotope which is gaining significant clinical attention in recent times is ^{68}Ga ($t_{1/2}$ = 68 min).[183−189] The convenient availability of this radioisotope from ^{68}Ge/^{68}Ga generators without the dependence on onsite cyclotrons makes it economical to use for a wide variety of PET scans. In particular, from the perspective of image-guided therapy, the radiolabeled peptides targeting somatostatin receptors, overexpressed in the majority of neuroendocrine malignancies, have a great potential for both imaging and therapy of tumors where other therapies fail.[185−189] The development of ^{68}Ga-labeled somatostatin analogues such as DOTANOC (DOTA-1-Nal^3-octreotide), DOTATOC (DOTA-D-Phe^1-Tyr^3-octreotide), or DOTATATE (DOTA-D-Phe^1-Tyr^3-Thr^8-octreotide) for PET/CT imaging has significantly improved the diagnosis of neuroendocrine tumors.[185] In a typical example, Gains et al. investigated the efficacy of PET/CT using ^{68}Ga-DOTATATE to select children with primary refractory or relapsed high-risk neuroblastoma for treatment with ^{177}Lu-DOTATATE and also evaluated whether this is a viable therapeutic option for those children.[190] Imaging with ^{68}Ga-DOTATATE could indicate the expression of somatostatin receptors and was of paramount importance for guiding radiotherapy (Figure 5A). Post-therapy of ^{177}Lu-DOTATATE, ^{68}Ga-DOTATATE scans was used to assess the response (Figure 5A), and a positive therapeutic outcome with a regression in some lesions and an apparent block of the metastatic activity could be observed in many cases. In a similar study, Budiawan et al. investigated the application and role of ^{68}Ga-DOTATATE PET/CT imaging in non-radioiodine-avid refractory thyroid cancer patients who have undergone peptide receptor radionuclide therapy (PRRT) with ^{90}Y/^{177}Lu-DOTATATE.[191] The authors concluded that PRRT guided by PET imaging is an effective therapeutic option with minimal toxicity, good response rate, and excellent survival benefits. In a different study, Wu et al. has reported the use of ^{68}Ga-labeled SIR spheres as PET imaging surrogate for distribution assessment and radiation dose estimation of ^{90}Y-SIR-Spheres, which are currently used in the treatment of solid liver tumors.[192,193] The authors observed that ^{68}Ga-SIR-Spheres had good *in vivo* stability and localization of the radiolabeled microparticles in the liver could be observed using PET imaging. Similar results were obtained by Avila-Rodriguez et al. on using ^{64}Cu or ^{86}Y labeled SIR spheres.[194]

Another example, close to clinical translation, is represented by PET imaging of human epidermal growth factor receptor 2 (HER2) expressions.[195] The overexpression of the HER2 is observed in ~15% of breast cancers and associated with poor prognosis in terms of overall survival.[196] Generally, ^{90}Y or ^{131}I labeled trastuzumab is used for targeted radiotherapy of primary or metastatic breast cancer, in experimental, preclinical, or clinical settings.[197] PET imaging of HER2- positive lesions in patients with metastatic breast cancer was reported by Dijkers et al.[198] The antibody trastuzumab was radiolabeled with ^{89}Zr, a PET imaging surrogate for ^{90}Y. Administration of ^{89}Zr-trastuzumab at appropriate doses allowed visualization and quantification of uptake in HER2-positive lesions in patients with metastatic breast cancer by PET (Figure 5B). The authors concluded that PET imaging of HER2 expression would aid in improving diagnosis, staging of the disease, guiding trastuzumab therapy, and monitoring the therapeutic response. A large number of other PET radiopharmaceuticals for molecular imaging and personalized cancer management have also been reported, details of which can be found in recent review articles.[199−223] We would apologize to those whose work could not be presented here, mainly due to the vastness of the field and availability of enormous literature which could not be summarized in a single review.

■ SUMMARY AND FUTURE PERSPECTIVES

In the last several decades, major milestones have been reached in every area of cancer care and a variety of anticancer drugs have been developed which are now commercially available worldwide.[224] Though most of these anticancer agents have the potential to be effective at sufficiently high doses, they are often associated with severe systemic side effects that cannot be tolerated by patients who are already weak due to effects of cancer. In a majority of the cases, the success of cancer therapy typically hinges upon circumventing the dose-limited toxicity while administering such drugs. Additionally, many conventional therapeutic agents often fail due to their limited ability to reach the target tissue and their poor selectivity against

cancerous lesions. Ideally a drug should possess perfect specificity to cancerous cells and have no effect on the rest of the body. To achieve these objectives, a variety of drug delivery systems have been engineered for the targeted delivery and controlled release of therapeutic agents to specifically kill the cancerous cells. The full potential of the drug delivery systems extends beyond treatment, and several image-guided approaches have now been implemented in areas ranging from new therapeutic target discovery to effectively monitoring tumor pharmacokinetics and drug distribution to modulation of drug release at the target site. In particular, PET image-guided drug delivery provides a means for treating a variety of diseases with minimal systemic involvement while concurrently monitoring therapeutic efficacy. This minimally invasive approach provides a comprehensive answer to many challenges with conventional therapeutic approaches and is expected to lead to a paradigm shift in cancer patient care.

The major advances in targeted drug delivery have been attributed to the recent progress in nanotechnology that has resulted in the development of nanosized drug delivery platforms having distinct advantages in cancer therapy. The versatile nanoplatforms provide opportunities for multifunctionalization so that a single platform can be used to detect and treat tumors, monitor treatment response, and thus guide therapeutic regimes. The nanoformulations can be functionalized to minimize clearance by the immune system and prolong circulation times, and also for attachment of suitable vectors (peptides, proteins, antibodies, etc.) targeting specific receptors, thereby enhancing tumor uptake through EPR effect as well as receptor-mediated endocytosis. The nanomaterial based delivery systems also result in improved treatment effects by protecting entrapped drugs from degradation during their delivery. The multifunctionality of the nanoplatforms offers possibility for multimodality molecular imaging. When two or more molecular imaging techniques are used in conjunction, they would provide synergistic information when compared with any single imaging modality. Additionally, multiple therapeutic agents such as chemotherapy, antiangiogenic, or gene therapy agents can be simultaneously delivered by nanocarriers to tumor sites to enhance the effectiveness of therapy.

Despite these advantages, it must be admitted that the field of PET image-guided drug delivery is still in its infancy and more systematic studies to understand the mechanisms for targeting and drug delivery would be required in order to translate these novel discoveries into clinical impact. The potential challenges to clinical translation of the drug delivery systems are *in vivo* characterization of the drug carriers, preclinical validation of targeting and delivery, studies of biodistribution, pharmacokinetics, pharmacodynamics, and toxicity, and scale-up manufacturing of delivery systems.[225−227]

Another major challenge lies in overcoming the biological barriers to deliver optimum amount of therapeutics into tumors and cells.[227] Moreover, the performance of the drug delivery carriers depends on several limiting factors which include the synthesis method adopted, their size and shape, internal structure of the drug carrier, drug loading methodology, surface functionalization and conjugation strategy adopted for attaching targeting ligands to the carrier platforms, etc., thereby making relative evaluation of different drug delivery platforms difficult. The issues related to toxicity of nanosized drug delivery platforms can be addressed by the use of biocompatible and biodegradable polymeric nanoparticles for drug delivery, which have received considerable attention in the recent times. Also, stimulus-responsive polymeric nanomaterials can be synthesized which mimic the behavior of biological molecules, where external stimuli or changes in local environment can trigger a change in property to regulate drug release. Such "smart" nanoparticle systems when coupled with suitable targeting ligands can probably best minimize off-target effects and maximize programmability, thereby offering the possibility of radically changing the practice of drug delivery.

While numerous obstacles face all new technologies, materializing the opportunities presented by PET image-guided drug delivery requires addressing the significant interdisciplinary challenges and biological barriers.[227] Besides these, several other complex factors, such as considerable regulatory hurdles, limited potential market, lobbying by the manufacturers of established anticancer drugs, lack of reimbursement strategies by the insurance agencies for such novel strategies, etc., might impede the "bench to bedside" translation of this promising approach. The concerted efforts of all stakeholders, which include scientists from academia as well as industries, progressive and technology savvy physicians, radiologists, surgeons, program advisory boards, regulatory authorities, and grant review panels, would be required, both to create enthusiasm for developing these new concepts and also to prevent adverse messaging based on myths, conjectures, hyperbole, and bias. This in turn would provide impetus to further research which might aid in clinical translation of PET image-guided drug delivery approaches and thus achieve the ultimate goal of "personalized medicine" in the near future.

AUTHOR INFORMATION

Corresponding Authors

*R.C.: Isotope Applications and Radiopharmaceuticals Division, Bhabha Atomic Research Centre, Mumbai 400085, India. Fax: +91-22-25505151. Phone: +91-22-25590624. E-mail: rubelc@barc.gov.in.

*W.C.: Departments of Radiology and Medical Physics, School of Medicine and Public Health, University of Wisconsin—Madison, Room 7137, 1111 Highland Ave, Madison, WI 53705-2275, United States. Fax: 1-608-265-0614. Phone: 1-608-262-1749. E-mail: wcai@uwhealth.org.

Notes

The authors declare no competing financial interest.

ACKNOWLEDGMENTS

This work is supported, in part, by the University of Wisconsin—Madison, the National Institutes of Health (NIBIB/NCI 1R01CA169365 and P30CA014520), the Department of Defense (W81XWH-11-1-0644), the American Cancer Society (125246-RSG-13-099-01-CCE), and the Fulbright Scholar Program (1831/FNPDR/2013).

REFERENCES

(1) Hatefi, A.; Minko, T. Advances in image-guided drug delivery. *Drug Delivery Transl. Res.* **2012**, *2*, 1−2.

(2) Gaidamakova, E. K.; Backer, M. V.; Backer, J. M. Molecular vehicle for target-mediated delivery of therapeutics and diagnostics. *J. Controlled Release* **2001**, *74*, 341−7.

(3) MacKay, J. A.; Li, Z. Theranostic agents that co-deliver therapeutic and imaging agents? *Adv. Drug Delivery Rev.* **2010**, *62*, 1003−4.

(4) Chow, E. K.; Ho, D. Cancer nanomedicine: from drug delivery to imaging. *Sci. Transl. Med.* **2013**, *5*, 216rv4.

(5) Solorio, L.; Patel, R. B.; Wu, H.; Krupka, T.; Exner, A. A. Advances in image-guided intratumoral drug delivery techniques. *Ther. Delivery* **2010**, *1*, 307−22.
(6) Fass, L. Imaging and cancer: a review. *Mol. Oncol.* **2008**, *2*, 115−52.
(7) Arias, J. L. Advanced methodologies to formulate nano-theragnostic agents for combined drug delivery and imaging. *Expert Opin. Drug Delivery* **2011**, *8*, 1589−608.
(8) Iyer, A. K.; He, J.; Amiji, M. M. Image-guided nanosystems for targeted delivery in cancer therapy. *Curr. Med. Chem.* **2012**, *19*, 3230−40.
(9) Terreno, E.; Uggeri, F.; Aime, S. Image guided therapy: the advent of theranostic agents. *J. Controlled Release* **2012**, *161*, 328−37.
(10) Zhang, Y.; Chan, H. F.; Leong, K. W. Advanced materials and processing for drug delivery: the past and the future. *Adv. Drug Delivery Rev.* **2013**, *65*, 104−20.
(11) Viness, P.; Pradeep, K.; Yahya, E. C. Cutting-edge techniques for molecular imaging with relevance to therapeutic delivery methods. In *Therapeutic Delivery Methods: A Concise Overview of Emerging Areas*; Future Science Ltd: London, 2013; pp 126−144.
(12) Bao, G.; Mitragotri, S.; Tong, S. Multifunctional nanoparticles for drug delivery and molecular imaging. *Annu. Rev. Biomed. Eng.* **2013**, *15*, 253−82.
(13) Malviya, G.; Nayak, T. K. PET Imaging to Monitor Cancer Therapy. *Curr. Pharm. Biotechnol.* **2013**, *14*, 669−82.
(14) Herschman, H. R. Molecular imaging: looking at problems, seeing solutions. *Science* **2003**, *302*, 605−8.
(15) Weissleder, R.; Pittet, M. J. Imaging in the era of molecular oncology. *Nature* **2008**, *452*, 580−9.
(16) Hoffman, J. M.; Gambhir, S. S. Molecular imaging: the vision and opportunity for radiology in the future. *Radiology* **2007**, *244*, 39−47.
(17) Berry, C. R.; Garg, P. Perspectives in molecular imaging through translational research, human medicine, and veterinary medicine. *Semin. Nucl. Med.* **2014**, *44*, 66−75.
(18) Jokerst, J. V.; Gambhir, S. S. Molecular imaging with theranostic nanoparticles. *Acc. Chem. Res.* **2011**, *44*, 1050−60.
(19) Ametamey, S. M.; Honer, M.; Schubiger, P. A. Molecular imaging with PET. *Chem. Rev.* **2008**, *108*, 1501−16.
(20) Jennings, L. E.; Long, N. J. 'Two is better than one'—probes for dual-modality molecular imaging. *Chem. Commun.* **2009**, 3511−24.
(21) Kiessling, F.; Fokong, S.; Bzyl, J.; Lederle, W.; Palmowski, M.; Lammers, T. Recent advances in molecular, multimodal and theranostic ultrasound imaging. *Adv. Drug Delivery Rev.* **2014**, *72*, 15−27, DOI: 10.1016/j.addr.2013.11.013.
(22) Song, Y.; Huang, Z.; Xu, J.; Ren, D.; Wang, Y.; Zheng, X.; Shen, Y.; Wang, L.; Gao, H.; Hou, J.; Pang, Z.; Qian, J.; Ge, J. Multimodal SPION-CREKA peptide based agents for molecular imaging of microthrombus in a rat myocardial ischemia-reperfusion model. *Biomaterials* **2014**, *35*, 2961−2970.
(23) Thorek, D. L.; Ulmert, D.; Diop, N. F.; Lupu, M. E.; Doran, M. G.; Huang, R.; Abou, D. S.; Larson, S. M.; Grimm, J. Non-invasive mapping of deep-tissue lymph nodes in live animals using a multimodal PET/MRI nanoparticle. *Nat. Commun.* **2014**, *5*, 3097.
(24) Basu, S. Personalized versus evidence-based medicine with PET-based imaging. *Nat. Rev. Clin. Oncol.* **2010**, *7*, 665−8.
(25) Bussink, J.; Kaanders, J. H.; van der Graaf, W. T.; Oyen, W. J. PET-CT for radiotherapy treatment planning and response monitoring in solid tumors. *Nat. Rev. Clin. Oncol.* **2011**, *8*, 233−42.
(26) Gambhir, S. S. Molecular imaging of cancer with positron emission tomography. *Nat. Rev. Cancer* **2002**, *2*, 683−93.
(27) Hicks, R. J.; Hofman, M. S. Is there still a role for SPECT-CT in oncology in the PET-CT era? *Nat. Rev. Clin. Oncol.* **2012**, *9*, 712−20.
(28) Cunha, L.; Szigeti, K.; Mathe, D.; Metello, L. F. The role of molecular imaging in modern drug development. *Drug Discovery Today* **2014**, DOI: 10.1016/j.drudis.2014.01.003, Epub ahead of print.
(29) Heskamp, S.; van Laarhoven, H. W.; van der Graaf, W. T.; Oyen, W. J.; Boerman, O. C. Radionuclide imaging of drug delivery for patient selection in targeted therapy. *Expert Opin. Drug Delivery* **2014**, *11*, 175−85.
(30) Jang, B. S. MicroSPECT and MicroPET Imaging of Small Animals for Drug Development. *Toxicol. Res.* **2013**, *29*, 1−6.
(31) Sharma, P.; Singh, H.; Basu, S.; Kumar, R. Positron emission tomography-computed tomography in the management of lung cancer: An update. *South Asian J. Cancer* **2013**, *2*, 171−8.
(32) van der Veldt, A. A.; Smit, E. F.; Lammertsma, A. A. Positron Emission Tomography as a Method for Measuring Drug Delivery to Tumors in vivo: The Example of [^{11}C]docetaxel. *Front. Oncol.* **2013**, *3*, 208.
(33) Lankveld, D. P.; Rayavarapu, R. G.; Krystek, P.; Oomen, A. G.; Verharen, H. W.; van Leeuwen, T. G.; De Jong, W. H.; Manohar, S. Blood clearance and tissue distribution of PEGylated and non-PEGylated gold nanorods after intravenous administration in rats. *Nanomedicine (London)* **2011**, *6*, 339−49.
(34) Larsen, E. K.; Nielsen, T.; Wittenborn, T.; Rydtoft, L. M.; Lokanathan, A. R.; Hansen, L.; Ostergaard, L.; Kingshott, P.; Howard, K. A.; Besenbacher, F.; Nielsen, N. C.; Kjems, J. Accumulation of magnetic iron oxide nanoparticles coated with variably sized polyethylene glycol in murine tumors. *Nanoscale* **2012**, *4*, 2352−61.
(35) Ohno, K.; Akashi, T.; Tsujii, Y.; Yamamoto, M.; Tabata, Y. Blood clearance and biodistribution of polymer brush-afforded silica particles prepared by surface-initiated living radical polymerization. *Biomacromolecules* **2012**, *13*, 927−36.
(36) Zhao, X.; Zhao, H.; Chen, Z.; Lan, M. Ultrasmall superparamagnetic iron oxide nanoparticles for magnetic resonance imaging contrast agent. *J. Nanosci. Nanotechnol.* **2014**, *14*, 210−20.
(37) Dong, H.; Dube, N.; Shu, J. Y.; Seo, J. W.; Mahakian, L. M.; Ferrara, K. W.; Xu, T. Long-circulating 15 nm micelles based on amphiphilic 3-helix peptide-PEG conjugates. *ACS Nano* **2012**, *6*, 5320−9.
(38) Gabizon, A.; Papahadjopoulos, D. Liposome formulations with prolonged circulation time in blood and enhanced uptake by tumors. *Proc. Natl. Acad. Sci. U.S.A.* **1988**, *85*, 6949−53.
(39) Liu, X.; Tao, H.; Yang, K.; Zhang, S.; Lee, S. T.; Liu, Z. Optimization of surface chemistry on single-walled carbon nanotubes for in vivo photothermal ablation of tumors. *Biomaterials* **2011**, *32*, 144−51.
(40) Lammers, T.; Kiessling, F.; Hennink, W. E.; Storm, G. Nanotheranostics and image-guided drug delivery: current concepts and future directions. *Mol. Pharmaceutics* **2010**, *7*, 1899−912.
(41) Janib, S. M.; Moses, A. S.; MacKay, J. A. Imaging and drug delivery using theranostic nanoparticles. *Adv. Drug Delivery Rev.* **2010**, *62*, 1052−63.
(42) Wilbur, D. S.; Pathare, P. M.; Hamlin, D. K.; Stayton, P. S.; To, R.; Klumb, L. A.; Buhler, K. R.; Vessella, R. L. Development of new biotin/streptavidin reagents for pretargeting. *Biomol. Eng.* **1999**, *16*, 113−8.
(43) Pene, F.; Courtine, E.; Cariou, A.; Mira, J. P. Toward theragnostics. *Crit. Care Med.* **2009**, *37*, S50−8.
(44) Liu, S. Bifunctional coupling agents for radiolabeling of biomolecules and target-specific delivery of metallic radionuclides. *Adv. Drug Delivery Rev.* **2008**, *60*, 1347−70.
(45) Bertrand, N.; Wu, J.; Xu, X.; Kamaly, N.; Farokhzad, O. C. Cancer nanotechnology: The impact of passive and active targeting in the era of modern cancer biology. *Adv. Drug Delivery Rev.* **2014**, *66*, 2−25.
(46) Ulrich, G.; Dudeck, O.; Furth, C.; Ruf, J.; Grosser, O. S.; Adolf, D.; Stiebler, M.; Ricke, J.; Amthauer, H. Predictive value of intratumoral ^{99m}Tc-macroaggregated albumin uptake in patients with colorectal liver metastases scheduled for radioembolization with ^{90}Y-microspheres. *J. Nucl. Med.* **2013**, *54*, 516−22.
(47) Elzoghby, A. O.; Samy, W. M.; Elgindy, N. A. Albumin-based nanoparticles as potential controlled release drug delivery systems. *J. Controlled Release* **2012**, *157*, 168−82.
(48) Misak, H. E.; Asmatulu, R.; Gopu, J. S.; Man, K. P.; Zacharias, N. M.; Wooley, P. H.; Yang, S. Y. Albumin-Based Nanocomposite

Spheres for Advanced Drug Delivery Systems. *Biotechnol. J.* **2014**, *9*, 163−70.
(49) Wu, Y.; Ihme, S.; Feuring-Buske, M.; Kuan, S. L.; Eisele, K.; Lamla, M.; Wang, Y.; Buske, C.; Weil, T. A core-shell albumin copolymer nanotransporter for high capacity loading and two-step release of doxorubicin with enhanced anti-leukemia activity. *Adv. Healthcare Mater.* **2013**, *2*, 884−94.
(50) Even, G. A.; Green, M. A. Gallium-68-labeled macroaggregated human serum albumin, ^{68}Ga-MAA. *Int. J. Radiat. Appl. Instrum. B* **1989**, *16*, 319−21.
(51) Okada, S.; Ohto, M.; Kuniyasu, Y.; Higashi, S.; Arimizu, N.; Uematsu, S. Estimation of the reticuloendothelial function by positron emission computed tomography (PET) study in chronic liver disease. *Nihon Shokakibyo Gakkai Zasshi* **1990**, *87*, 90−9.
(52) Maus, S.; Buchholz, H. G.; Ament, S.; Brochhausen, C.; Bausbacher, N.; Schreckenberger, M. Labelling of commercially available human serum albumin kits with ^{68}Ga as surrogates for ^{99m}Tc-MAA microspheres. *Appl. Radiat. Isot.* **2011**, *69*, 171−5.
(53) Geschwind, J. F.; Salem, R.; Carr, B. I.; Soulen, M. C.; Thurston, K. G.; Goin, K. A.; Van Buskirk, M.; Roberts, C. A.; Goin, J. E. Yttrium-90 microspheres for the treatment of hepatocellular carcinoma. *Gastroenterology* **2004**, *127*, S194−205.
(54) Kennedy, A. S.; Salem, R. Radioembolization (yttrium-90 microspheres) for primary and metastatic hepatic malignancies. *Cancer J.* **2010**, *16*, 163−75.
(55) Murthy, R.; Nunez, R.; Szklaruk, J.; Erwin, W.; Madoff, D. C.; Gupta, S.; Ahrar, K.; Wallace, M. J.; Cohen, A.; Coldwell, D. M.; Kennedy, A. S.; Hicks, M. E. Yttrium-90 microsphere therapy for hepatic malignancy: devices, indications, technical considerations, and potential complications. *Radiographics* **2005**, *25* (Suppl. 1), S41−55.
(56) Liao, A. H.; Wu, S. Y.; Wang, H. E.; Weng, C. H.; Wu, M. F.; Li, P. C. Evaluation of ^{18}F-labeled targeted perfluorocarbon-filled albumin microbubbles as a probe for microUS and microPET in tumor-bearing mice. *Ultrasonics* **2013**, *53*, 320−7.
(57) Goyal, P.; Goyal, K.; Vijaya Kumar, S. G.; Singh, A.; Katare, O. P.; Mishra, D. N. Liposomal drug delivery systems—clinical applications. *Acta Pharm.* **2005**, *55*, 1−25.
(58) Medina, O. P.; Zhu, Y.; Kairemo, K. Targeted liposomal drug delivery in cancer. *Curr. Pharm. Des* **2004**, *10*, 2981−9.
(59) Petersen, A. L.; Hansen, A. E.; Gabizon, A.; Andresen, T. L. Liposome imaging agents in personalized medicine. *Adv. Drug Delivery Rev.* **2012**, *64*, 1417−35.
(60) Klibanov, A. L.; Maruyama, K.; Torchilin, V. P.; Huang, L. Amphipathic polyethyleneglycols effectively prolong the circulation time of liposomes. *FEBS Lett.* **1990**, *268*, 235−7.
(61) O'Shaughnessy, J. A. Pegylated liposomal doxorubicin in the treatment of breast cancer. *Clin. Breast Cancer* **2003**, *4*, 318−28.
(62) Torchilin, V. P.; Omelyanenko, V. G.; Papisov, M. I.; Bogdanov, A. A., Jr.; Trubetskoy, V. S.; Herron, J. N.; Gentry, C. A. Poly(ethylene glycol) on the liposome surface: on the mechanism of polymer-coated liposome longevity. *Biochim. Biophys. Acta* **1994**, *1195*, 11−20.
(63) Seo, J. W.; Zhang, H.; Kukis, D. L.; Meares, C. F.; Ferrara, K. W. A novel method to label preformed liposomes with ^{64}Cu for positron emission tomography (PET) imaging. *Bioconjugate Chem.* **2008**, *19*, 2577−84.
(64) Seo, J. W.; Mahakian, L. M.; Kheirolomoom, A.; Zhang, H.; Meares, C. F.; Ferdani, R.; Anderson, C. J.; Ferrara, K. W. Liposomal Cu-64 labeling method using bifunctional chelators: poly(ethylene glycol) spacer and chelator effects. *Bioconjugate Chem.* **2010**, *21*, 1206−15.
(65) Seo, J. W.; Qin, S.; Mahakian, L. M.; Watson, K. D.; Kheirolomoom, A.; Ferrara, K. W. Positron emission tomography imaging of the stability of Cu-64 labeled dipalmitoyl and distearoyl lipids in liposomes. *J. Controlled Release* **2011**, *151*, 28−34.
(66) Petersen, A. L.; Binderup, T.; Rasmussen, P.; Henriksen, J. R.; Elema, D. R.; Kjaer, A.; Andresen, T. L. ^{64}Cu loaded liposomes as positron emission tomography imaging agents. *Biomaterials* **2011**, *32*, 2334−41.
(67) Petersen, A. L.; Binderup, T.; Jolck, R. I.; Rasmussen, P.; Henriksen, J. R.; Pfeifer, A. K.; Kjaer, A.; Andresen, T. L. Positron emission tomography evaluation of somatostatin receptor targeted ^{64}Cu-TATE-liposomes in a human neuroendocrine carcinoma mouse model. *J. Controlled Release* **2012**, *160*, 254−63.
(68) Sowa-Staszczak, A.; Hubalewska-Dydejczyk, A.; Tomaszuk, M. PRRT as neoadjuvant treatment in NET. *Recent Results Cancer Res.* **2013**, *194*, 479−85.
(69) Allavena, P.; Sica, A.; Solinas, G.; Porta, C.; Mantovani, A. The inflammatory micro-environment in tumor progression: the role of tumor-associated macrophages. *Crit Rev. Oncol. Hematol.* **2008**, *66*, 1−9.
(70) Fukuda, K.; Kobayashi, A.; Watabe, K. The role of tumor-associated macrophage in tumor progression. *Front. Biosci., Scholar Ed.* **2012**, *4*, 787−98.
(71) Locke, L. W.; Mayo, M. W.; Yoo, A. D.; Williams, M. B.; Berr, S. S. PET imaging of tumor associated macrophages using mannose coated ^{64}Cu liposomes. *Biomaterials* **2012**, *33*, 7785−93.
(72) Urakami, T.; Akai, S.; Katayama, Y.; Harada, N.; Tsukada, H.; Oku, N. Novel amphiphilic probes for [^{18}F]-radiolabeling preformed liposomes and determination of liposomal trafficking by positron emission tomography. *J. Med. Chem.* **2007**, *50*, 6454−7.
(73) Urakami, T.; Kawaguchi, A. T.; Akai, S.; Hatanaka, K.; Koide, H.; Shimizu, K.; Asai, T.; Fukumoto, D.; Harada, N.; Tsukada, H.; Oku, N. In vivo distribution of liposome-encapsulated hemoglobin determined by positron emission tomography. *Artif. Organs* **2009**, *33*, 164−8.
(74) Marik, J.; Tartis, M. S.; Zhang, H.; Fung, J. Y.; Kheirolomoom, A.; Sutcliffe, J. L.; Ferrara, K. W. Long-circulating liposomes radiolabeled with [^{18}F]fluorodipalmitin ([^{18}F]FDP). *Nucl. Med. Biol.* **2007**, *34*, 165−71.
(75) Paoli, E. E.; Kruse, D. E.; Seo, J. W.; Zhang, H.; Kheirolomoom, A.; Watson, K. D.; Chiu, P.; Stahlberg, H.; Ferrara, K. W. An optical and microPET assessment of thermally-sensitive liposome biodistribution in the Met-1 tumor model: Importance of formulation. *J. Controlled Release* **2010**, *143*, 13−22.
(76) Oku, N.; Yamashita, M.; Katayama, Y.; Urakami, T.; Hatanaka, K.; Shimizu, K.; Asai, T.; Tsukada, H.; Akai, S.; Kanazawa, H. PET imaging of brain cancer with positron emitter-labeled liposomes. *Int. J. Pharm.* **2011**, *403*, 170−7.
(77) Mitchell, N.; Kalber, T. L.; Cooper, M. S.; Sunassee, K.; Chalker, S. L.; Shaw, K. P.; Ordidge, K. L.; Badar, A.; Janes, S. M.; Blower, P. J.; Lythgoe, M. F.; Hailes, H. C.; Tabor, A. B. Incorporation of paramagnetic, fluorescent and PET/SPECT contrast agents into liposomes for multimodal imaging. *Biomaterials* **2013**, *34*, 1179−92.
(78) Lavasanifar, A.; Samuel, J.; Kwon, G. S. Poly(ethylene oxide)-block-poly(L-amino acid) micelles for drug delivery. *Adv. Drug Delivery Rev.* **2002**, *54*, 169−90.
(79) Wei, T.; Liu, J.; Ma, H.; Cheng, Q.; Huang, Y.; Zhao, J.; Huo, S.; Xue, X.; Liang, Z.; Liang, X. J. Functionalized nanoscale micelles improve drug delivery for cancer therapy in vitro and in vivo. *Nano Lett.* **2013**, *13*, 2528−34.
(80) Kedar, U.; Phutane, P.; Shidhaye, S.; Kadam, V. Advances in polymeric micelles for drug delivery and tumor targeting. *Nanomedicine* **2010**, *6*, 714−29.
(81) Mackiewicz, N.; Gravel, E.; Garofalakis, A.; Ogier, J.; John, J.; Dupont, D. M.; Gombert, K.; Tavitian, B.; Doris, E.; Duconge, F. Tumor-targeted polydiacetylene micelles for in vivo imaging and drug delivery. *Small* **2011**, *7*, 2786−92.
(82) Cho, H.; Lai, T. C.; Kwon, G. S. Poly(ethylene glycol)-block-poly(epsilon-caprolactone) micelles for combination drug delivery: evaluation of paclitaxel, cyclopamine and gossypol in intraperitoneal xenograft models of ovarian cancer. *J. Controlled Release* **2013**, *166*, 1−9.
(83) Morris, P. G.; Abrey, L. E. Novel targeted agents for platelet-derived growth factor receptor and c-KIT in malignant gliomas. *Target Oncol.* **2010**, *5*, 193−200.
(84) Benezra, M.; Hambardzumyan, D.; Penate-Medina, O.; Veach, D. R.; Pillarsetty, N.; Smith-Jones, P.; Phillips, E.; Ozawa, T.;

Zanzonico, P. B.; Longo, V.; Holland, E. C.; Larson, S. M.; Bradbury, M. S. Fluorine-labeled dasatinib nanoformulations as targeted molecular imaging probes in a PDGFB-driven murine glioblastoma model. *Neoplasia* **2012**, *14*, 1132−43.
(85) Oerlemans, C.; Bult, W.; Bos, M.; Storm, G.; Nijsen, J. F.; Hennink, W. E. Polymeric micelles in anticancer therapy: targeting, imaging and triggered release. *Pharm. Res.* **2010**, *27*, 2569−89.
(86) Xiao, Y.; Hong, H.; Javadi, A.; Engle, J. W.; Xu, W.; Yang, Y.; Zhang, Y.; Barnhart, T. E.; Cai, W.; Gong, S. Multifunctional unimolecular micelles for cancer-targeted drug delivery and positron emission tomography imaging. *Biomaterials* **2012**, *33*, 3071−82.
(87) Guo, J.; Hong, H.; Chen, G.; Shi, S.; Zheng, Q.; Zhang, Y.; Theuer, C. P.; Barnhart, T. E.; Cai, W.; Gong, S. Image-guided and tumor-targeted drug delivery with radiolabeled unimolecular micelles. *Biomaterials* **2013**, *34*, 8323−32.
(88) Xu, G.; McLeod, H. L. Strategies for enzyme/prodrug cancer therapy. *Clin. Cancer Res.* **2001**, *7*, 3314−24.
(89) Tong, X.; Chen, X.; Li, C. Imaging beyond the diagnosis: image-guided enzyme/prodrug cancer therapy. *Acta Biochim. Biophys. Sin. (Shanghai)* **2011**, *43*, 4−12.
(90) Li, C.; Penet, M. F.; Winnard, P., Jr.; Artemov, D.; Bhujwalla, Z. M. Image-guided enzyme/prodrug cancer therapy. *Clin. Cancer Res.* **2008**, *14*, 515−22.
(91) Springer, C. J.; Niculescu-Duvaz, I. I. Antibody-directed enzyme prodrug therapy (ADEPT): a review. *Adv. Drug Delivery Rev.* **1997**, *26*, 151−172.
(92) Bagshawe, K. D.; Sharma, S. K.; Burke, P. J.; Melton, R. G.; Knox, R. J. Developments with targeted enzymes in cancer therapy. *Curr. Opin. Immunol* **1999**, *11*, 579−83.
(93) Silva, A. T.; Chung, M. C.; Castro, L. F.; Guido, R. V.; Ferreira, E. I. Advances in prodrug design. *Mini-Rev. Med. Chem.* **2005**, *5*, 893−914.
(94) Bhaumik, S. Advances in imaging gene-directed enzyme prodrug therapy. *Curr. Pharm. Biotechnol.* **2011**, *12*, 497−507.
(95) Szabo, Z.; Xia, J.; Mathews, W. B.; Brown, P. R. Future direction of renal positron emission tomography. *Semin. Nucl. Med.* **2006**, *36*, 36−50.
(96) Wunderbaldinger, P.; Bogdanov, A.; Weissleder, R. New approaches for imaging in gene therapy. *Eur. J. Radiol.* **2000**, *34*, 156−65.
(97) Bankiewicz, K. S.; Eberling, J. L.; Kohutnicka, M.; Jagust, W.; Pivirotto, P.; Bringas, J.; Cunningham, J.; Budinger, T. F.; Harvey-White, J. Convection-enhanced delivery of AAV vector in parkinsonian monkeys; in vivo detection of gene expression and restoration of dopaminergic function using pro-drug approach. *Exp. Neurol.* **2000**, *164*, 2−14.
(98) Jacobs, A.; Voges, J.; Reszka, R.; Lercher, M.; Gossmann, A.; Kracht, L.; Kaestle, C.; Wagner, R.; Wienhard, K.; Heiss, W. D. Positron-emission tomography of vector-mediated gene expression in gene therapy for gliomas. *Lancet* **2001**, *358*, 727−9.
(99) Hackman, T.; Doubrovin, M.; Balatoni, J.; Beresten, T.; Ponomarev, V.; Beattie, B.; Finn, R.; Bornmann, W.; Blasberg, R.; Tjuvajev, J. G. Imaging expression of cytosine deaminase-herpes virus thymidine kinase fusion gene (CD/TK) expression with [^{124}I]FIAU and PET. *Mol. Imaging* **2002**, *1*, 36−42.
(100) Malik, N.; Luthra, S. K.; Burke, P.; Price, P. M.; Aboagye, E. O.; Latigo, J.; Zhao, Y.; Brady, F. Radiosynthesis of 4-[(2-chloroethyl)(2-[11C]ethyl)amino]-phenoxycarbonyl-l-glutamic acid a half mustard prodrug as a potential probe for imaging antibody- and gene-directed enzyme prodrug therapy with positron emission tomography. *Appl. Radiat. Isot.* **2004**, *60*, 825−834.
(101) Eiseman, J. L.; Brown-Proctor, C.; Kinahan, P. E.; Collins, J. M.; Anderson, L. W.; Joseph, E.; Hamburger, D. R.; Pan, S. S.; Mathis, C. A.; Egorin, M. J.; Klecker, R. W. Distribution of 1-(2-deoxy-2-fluoro-beta-D-arabinofuranosyl) uracil in mice bearing colorectal cancer xenografts: rationale for therapeutic use and as a positron emission tomography probe for thymidylate synthase. *Clin. Cancer Res.* **2004**, *10*, 6669−76.
(102) Tseng, J. C.; Zanzonico, P. B.; Levin, B.; Finn, R.; Larson, S. M.; Meruelo, D. Tumor-specific in vivo transfection with HSV-1 thymidine kinase gene using a Sindbis viral vector as a basis for prodrug ganciclovir activation and PET. *J. Nucl. Med.* **2006**, *47*, 1136−43.
(103) Stelter, L.; Tseng, J. C.; Torosjan, A.; Levin, B.; Longo, V. A.; Pillarsetty, N.; Zanzonico, P.; Meruelo, D.; Larson, S. M. Tumor-specific targeting with modified Sindbis viral vectors: evaluation with optical imaging and positron emission tomography in vivo. *Mol. Imaging Biol.* **2013**, *15*, 166−74.
(104) Wang, H. E.; Yu, H. M.; Liu, R. S.; Lin, M.; Gelovani, J. G.; Hwang, J. J.; Wei, H. J.; Deng, W. P. Molecular imaging with ^{123}I-FIAU, ^{18}F-FUdR, ^{18}F-FET, and ^{18}F-FDG for monitoring herpes simplex virus type 1 thymidine kinase and ganciclovir prodrug activation gene therapy of cancer. *J. Nucl. Med.* **2006**, *47*, 1161−71.
(105) Antunes, I. F.; Haisma, H. J.; Elsinga, P. H.; Dierckx, R. A.; de Vries, E. F. Synthesis and evaluation of [^{18}F]-FEAnGA as a PET Tracer for beta-glucuronidase activity. *Bioconjugate Chem.* **2010**, *21*, 911−20.
(106) Antunes, I. F.; Haisma, H. J.; Elsinga, P. H.; van Waarde, A.; Willemsen, A. T.; Dierckx, R. A.; de Vries, E. F. In vivo evaluation of 1-O-(4-(2-fluoroethyl-carbamoyloxymethyl)-2-nitrophenyl)-O-beta-D-glucopyronurona te: a positron emission tomographic tracer for imaging beta-glucuronidase activity in a tumor/inflammation rodent model. *Mol. Imaging* **2012**, *11*, 77−87.
(107) Antunes, I. F.; Haisma, H. J.; Elsinga, P. H.; Di Gialleonardo, V.; van Waarde, A.; Willemsen, A. T.; Dierckx, R. A.; de Vries, E. F. Induction of beta-glucuronidase release by cytostatic agents in small tumors. *Mol. Pharmaceutics* **2012**, *9*, 3277−85.
(108) Moon, B. S.; Jang, S. J.; Kim, S. J.; Lee, T. S.; Chi, D. Y.; Lee, B. C.; Kang, J. H.; Kim, S. E. Synthesis and evaluation of a 18F-labeled 4-ipomeanol as an imaging agent for CYP4B1 gene prodrug activation therapy. *Cancer Biother. Radiopharm.* **2013**, *28*, 588−97.
(109) Zhu, Q.; Talton, J.; Zhang, G.; Cunningham, T.; Wang, Z.; Waters, R. C.; Kirk, J.; Eppler, B.; Klinman, D. M.; Sui, Y.; Gagnon, S.; Belyakov, I. M.; Mumper, R. J.; Berzofsky, J. A. Large intestine-targeted, nanoparticle-releasing oral vaccine to control genitorectal viral infection. *Nat. Med.* **2012**, *18*, 1291−6.
(110) Kochut, A.; Dersch, P. Bacterial invasion factors: tools for crossing biological barriers and drug delivery? *Eur. J. Pharm. Biopharm.* **2013**, *84*, 242−50.
(111) Zhao, Y.; Trewyn, B. G.; Slowing, I. I.; Lin, V. S. Mesoporous silica nanoparticle-based double drug delivery system for glucose-responsive controlled release of insulin and cyclic AMP. *J. Am. Chem. Soc.* **2009**, *131*, 8398−400.
(112) Patil, Y. B.; Swaminathan, S. K.; Sadhukha, T.; Ma, L.; Panyam, J. The use of nanoparticle-mediated targeted gene silencing and drug delivery to overcome tumor drug resistance. *Biomaterials* **2010**, *31*, 358−65.
(113) Fang, W.; Yang, J.; Gong, J.; Zheng, N. Photo- and pH-Triggered Release of Anticancer Drugs from Mesoporous Silica-Coated Pd@Ag Nanoparticles. *Adv. Funct Mater.* **2012**, *22*, 842−848.
(114) Klichko, Y.; Liong, M.; Choi, E.; Angelos, S.; Nel, A. E.; Stoddart, J. F.; Tamanoi, F.; Zink, J. I. Mesostructured Silica for Optical Functionality, Nanomachines, and Drug Delivery. *J. Am. Ceram. Soc.* **2009**, *92*, s2−s10.
(115) Kim, J. H.; Noh, Y. W.; Heo, M. B.; Cho, M. Y.; Lim, Y. T. Multifunctional hybrid nanoconjugates for efficient in vivo delivery of immunomodulating oligonucleotides and enhanced antitumor immunity. *Angew. Chem., Int. Ed.* **2012**, *51*, 9670−3.
(116) Bagalkot, V.; Gao, X. siRNA-aptamer chimeras on nanoparticles: preserving targeting functionality for effective gene silencing. *ACS Nano* **2011**, *5*, 8131−9.
(117) Sardesai, N. P.; Barron, J. C.; Rusling, J. F. Carbon nanotube microwell array for sensitive electrochemiluminescent detection of cancer biomarker proteins. *Anal. Chem.* **2011**, *83*, 6698−703.
(118) Chen, T.; Shukoor, M. I.; Wang, R.; Zhao, Z.; Yuan, Q.; Bamrungsap, S.; Xiong, X.; Tan, W. Smart multifunctional

nanostructure for targeted cancer chemotherapy and magnetic resonance imaging. *ACS Nano* **2011**, *5*, 7866−73.
(119) Gao, Y.; Yang, C.; Liu, X.; Ma, R.; Kong, D.; Shi, L. A multifunctional nanocarrier based on nanogated mesoporous silica for enhanced tumor-specific uptake and intracellular delivery. *Macromol. Biosci.* **2012**, *12*, 251−9.
(120) Xia, T.; Kovochich, M.; Liong, M.; Meng, H.; Kabehie, S.; George, S.; Zink, J. I.; Nel, A. E. Polyethyleneimine coating enhances the cellular uptake of mesoporous silica nanoparticles and allows safe delivery of siRNA and DNA constructs. *ACS Nano* **2009**, *3*, 3273−86.
(121) Li, J.; Gupta, S.; Li, C. Research perspectives: gold nanoparticles in cancer theranostics. *Quant. Imaging Med. Surg.* **2013**, *3*, 284−91.
(122) Liboiron, B. D.; Mayer, L. D. Nanoscale particulate systems for multidrug delivery: towards improved combination chemotherapy. *Ther. Delivery* **2014**, *5*, 149−71.
(123) Sanchez-Dominguez, C. N.; Gallardo-Blanco, H. L.; Rodriguez-Rodriguez, A. A.; Vela-Gonzalez, A. V.; Sanchez-Dominguez, M. Nanoparticles vs cancer: a multifuncional tool. *Curr. Top. Med. Chem.* **2014**, *14*, 664−75.
(124) Long, N. V.; Thi, C. M.; Yong, Y.; Cao, Y.; Nogami, M. Synthesis and Characterization of Fe-Based Metal and Oxide Based Nanoparticles: Discoveries and Research Highlights of Potential Applications in Biology and Medicine. *Recent Pat. Nanotechnol.* **2014**, *8*, 52−61.
(125) Lepeltier, E.; Bourgaux, C.; Couvreur, P. Nanoprecipitation and the "Ouzo effect": Application to drug delivery devices. *Adv. Drug Delivery Rev.* **2014**, *71*, 86−97, DOI: 10.1016/j.addr.2013.12.009.
(126) Bhattacharya, R.; Mukherjee, P.; Xiong, Z.; Atala, A.; Soker, S.; Mukhopadhyay, D. Gold Nanoparticles Inhibit VEGF165-Induced Proliferation of HUVEC Cells. *Nano Lett.* **2004**, *4*, 2479−81.
(127) Kogan, M. J.; Olmedo, I.; Hosta, L.; Guerrero, A. R.; Cruz, L. J.; Albericio, F. Peptides and metallic nanoparticles for biomedical applications. *Nanomedicine (London)* **2007**, *2*, 287−306.
(128) Hosta-Rigau, L.; Olmedo, I.; Arbiol, J.; Cruz, L. J.; Kogan, M. J.; Albericio, F. Multifunctionalized gold nanoparticles with peptides targeted to gastrin-releasing peptide receptor of a tumor cell line. *Bioconjugate Chem.* **2010**, *21*, 1070−8.
(129) Hosta, L.; Pla-Roca, M.; Arbiol, J.; Lopez-Iglesias, C.; Samitier, J.; Cruz, L. J.; Kogan, M. J.; Albericio, F. Conjugation of Kahalalide F with gold nanoparticles to enhance in vitro antitumoral activity. *Bioconjugate Chem.* **2009**, *20*, 138−46.
(130) Guerrero, S.; Herance, J. R.; Rojas, S.; Mena, J. F.; Gispert, J. D.; Acosta, G. A.; Albericio, F.; Kogan, M. J. Synthesis and in vivo evaluation of the biodistribution of a ^{18}F-labeled conjugate gold-nanoparticle-peptide with potential biomedical application. *Bioconjugate Chem.* **2012**, *23*, 399−408.
(131) Kuo, W. S.; Chang, C. N.; Chang, Y. T.; Yang, M. H.; Chien, Y. H.; Chen, S. J.; Yeh, C. S. Gold nanorods in photodynamic therapy, as hyperthermia agents, and in near-infrared optical imaging. *Angew. Chem., Int. Ed.* **2010**, *49*, 2711−5.
(132) Xiao, Y.; Hong, H.; Matson, V. Z.; Javadi, A.; Xu, W.; Yang, Y.; Zhang, Y.; Engle, J. W.; Nickles, R. J.; Cai, W.; Steeber, D. A.; Gong, S. Gold Nanorods Conjugated with Doxorubicin and cRGD for Combined Anticancer Drug Delivery and PET Imaging. *Theranostics* **2012**, *2*, 757−68.
(133) Xie, H.; Diagaradjane, P.; Deorukhkar, A. A.; Goins, B.; Bao, A.; Phillips, W. T.; Wang, Z.; Schwartz, J.; Krishnan, S. Integrin $\alpha_v\beta_3$-targeted gold nanoshells augment tumor vasculature-specific imaging and therapy. *Int. J. Nanomedicine* **2011**, *6*, 259−69.
(134) Kwon, S.; Singh, R. K.; Perez, R. A.; Abou Neel, E. A.; Kim, H. W.; Chrzanowski, W. Silica-based mesoporous nanoparticles for controlled drug delivery. *J. Tissue Eng.* **2013**, DOI: 10.1177/2041731413503357.
(135) Turcheniuk, K.; Tarasevych, A. V.; Kukhar, V. P.; Boukherroub, R.; Szunerits, S. Recent advances in surface chemistry strategies for the fabrication of functional iron oxide based magnetic nanoparticles. *Nanoscale* **2013**, *5*, 10729−52.
(136) Benezra, M.; Penate-Medina, O.; Zanzonico, P. B.; Schaer, D.; Ow, H.; Burns, A.; DeStanchina, E.; Longo, V.; Herz, E.; Iyer, S.; Wolchok, J.; Larson, S. M.; Wiesner, U.; Bradbury, M. S. Multimodal silica nanoparticles are effective cancer-targeted probes in a model of human melanoma. *J. Clin. Invest.* **2011**, *121*, 2768−80.
(137) Burns, A. A.; Vider, J.; Ow, H.; Herz, E.; Penate-Medina, O.; Baumgart, M.; Larson, S. M.; Wiesner, U.; Bradbury, M. Fluorescent silica nanoparticles with efficient urinary excretion for nanomedicine. *Nano Lett.* **2009**, *9*, 442−8.
(138) US FDA. Investigational New Drug approval for first-in-human trial of novel cancer-targeting nanoparticle. News & Analysis. *Ther. Delivery* **2011**, *2*, 287.
(139) Tang, L.; Yang, X.; Dobrucki, L. W.; Chaudhury, I.; Yin, Q.; Yao, C.; Lezmi, S.; Helferich, W. G.; Fan, T. M.; Cheng, J. Aptamer-functionalized, ultra-small, monodisperse silica nanoconjugates for targeted dual-modal imaging of lymph nodes with metastatic tumors. *Angew. Chem., Int. Ed.* **2012**, *51*, 12721−6.
(140) Kim, J. S.; Kim, Y. H.; Kim, J. H.; Kang, K. W.; Tae, E. L.; Youn, H.; Kim, D.; Kim, S. K.; Kwon, J. T.; Cho, M. H.; Lee, Y. S.; Jeong, J. M.; Chung, J. K.; Lee, D. S. Development and in vivo imaging of a PET/MRI nanoprobe with enhanced NIR fluorescence by dye encapsulation. *Nanomedicine (London)* **2012**, *7*, 219−29.
(141) Di Pasqua, A. J.; Yuan, H.; Chung, Y.; Kim, J. K.; Huckle, J. E.; Li, C.; Sadgrove, M.; Tran, T. H.; Jay, M.; Lu, X. Neutron-activatable holmium-containing mesoporous silica nanoparticles as a potential radionuclide therapeutic agent for ovarian cancer. *J. Nucl. Med.* **2013**, *54*, 111−6.
(142) Chen, F.; Hong, H.; Zhang, Y.; Valdovinos, H. F.; Shi, S.; Kwon, G. S.; Theuer, C. P.; Barnhart, T. E.; Cai, W. In vivo tumor targeting and image-guided drug delivery with antibody-conjugated, radiolabeled mesoporous silica nanoparticles. *ACS Nano* **2013**, *7*, 9027−39.
(143) Choi, J. S.; Park, J. C.; Nah, H.; Woo, S.; Oh, J.; Kim, K. M.; Cheon, G. J.; Chang, Y.; Yoo, J.; Cheon, J. A hybrid nanoparticle probe for dual-modality positron emission tomography and magnetic resonance imaging. *Angew. Chem., Int. Ed.* **2008**, *47*, 6259−62.
(144) Xu, C.; Xie, J.; Ho, D.; Wang, C.; Kohler, N.; Walsh, E. G.; Morgan, J. R.; Chin, Y. E.; Sun, S. Au-Fe_3O_4 dumbbell nanoparticles as dual-functional probes. *Angew. Chem., Int. Ed.* **2008**, *47*, 173−6.
(145) Lee, S.; Chen, X. Dual-modality probes for in vivo molecular imaging. *Mol. Imaging* **2009**, *8*, 87−100.
(146) Xie, J.; Huang, J.; Li, X.; Sun, S.; Chen, X. Iron oxide nanoparticle platform for biomedical applications. *Curr. Med. Chem.* **2009**, *16*, 1278−94.
(147) Xie, J.; Chen, K.; Huang, J.; Lee, S.; Wang, J.; Gao, J.; Li, X.; Chen, X. PET/NIRF/MRI triple functional iron oxide nanoparticles. *Biomaterials* **2010**, *31*, 3016−22.
(148) Chen, F.; Ellison, P. A.; Lewis, C. M.; Hong, H.; Zhang, Y.; Shi, S.; Hernandez, R.; Meyerand, M. E.; Barnhart, T. E.; Cai, W. Chelator-free synthesis of a dual-modality PET/MRI agent. *Angew. Chem., Int. Ed.* **2013**, *52*, 13319−23.
(149) Chakravarty, R.; Ram, R.; Jagdeesan, K. C.; Venkatesh, M.; Dash, A. Polymer Embedded Nanocrystalline Titania: A New Generation Sorbent for the Separation of ^{77}As from Ge for Biomedical Applications. *Chromatographia* **2011**, *74*, 531−540.
(150) Yang, X.; Hong, H.; Grailer, J. J.; Rowland, I. J.; Javadi, A.; Hurley, S. A.; Xiao, Y.; Yang, Y.; Zhang, Y.; Nickles, R. J.; Cai, W.; Steeber, D. A.; Gong, S. cRGD-functionalized, DOX-conjugated, and ^{64}Cu-labeled superparamagnetic iron oxide nanoparticles for targeted anticancer drug delivery and PET/MR imaging. *Biomaterials* **2011**, *32*, 4151−60.
(151) Peer, D.; Karp, J. M.; Hong, S.; Farokhzad, O. C.; Margalit, R.; Langer, R. Nanocarriers as an emerging platform for cancer therapy. *Nat. Nanotechnol.* **2007**, *2*, 751−60.
(152) Bartlett, D. W.; Su, H.; Hildebrandt, I. J.; Weber, W. A.; Davis, M. E. Impact of tumor-specific targeting on the biodistribution and efficacy of siRNA nanoparticles measured by multimodality in vivo imaging. *Proc. Natl. Acad. Sci. U.S.A.* **2007**, *104*, 15549−54.

(153) Rossin, R.; Muro, S.; Welch, M. J.; Muzykantov, V. R.; Schuster, D. P. In vivo imaging of ^{64}Cu-labeled polymer nanoparticles targeted to the lung endothelium. *J. Nucl. Med.* **2008**, *49*, 103−11.
(154) Simone, E. A.; Zern, B. J.; Chacko, A. M.; Mikitsh, J. L.; Blankemeyer, E. R.; Muro, S.; Stan, R. V.; Muzykantov, V. R. Endothelial targeting of polymeric nanoparticles stably labeled with the PET imaging radioisotope iodine-124. *Biomaterials* **2012**, *33*, 5406−13.
(155) Zhu, Z.; Li, Y.; Li, X.; Li, R.; Jia, Z.; Liu, B.; Guo, W.; Wu, W.; Jiang, X. Paclitaxel-loaded poly(N-vinylpyrrolidone)-b-poly(epsilon-caprolactone) nanoparticles: preparation and antitumor activity in vivo. *J. Controlled Release* **2010**, *142*, 438−46.
(156) Liu, Q.; Li, R.; Zhu, Z.; Qian, X.; Guan, W.; Yu, L.; Yang, M.; Jiang, X.; Liu, B. Enhanced antitumor efficacy, biodistribution and penetration of docetaxel-loaded biodegradable nanoparticles. *Int. J. Pharm.* **2012**, *430*, 350−8.
(157) Zhou, J.; Patel, T. R.; Sirianni, R. W.; Strohbehn, G.; Zheng, M. Q.; Duong, N.; Schafbauer, T.; Huttner, A. J.; Huang, Y.; Carson, R. E.; Zhang, Y.; Sullivan, D. J., Jr.; Piepmeier, J. M.; Saltzman, W. M. Highly penetrative, drug-loaded nanocarriers improve treatment of glioblastoma. *Proc. Natl. Acad. Sci. U.S.A.* **2013**, *110*, 11751−6.
(158) Chen, K. J.; Tang, L.; Garcia, M. A.; Wang, H.; Lu, H.; Lin, W. Y.; Hou, S.; Yin, Q.; Shen, C. K.; Cheng, J.; Tseng, H. R. The therapeutic efficacy of camptothecin-encapsulated supramolecular nanoparticles. *Biomaterials* **2012**, *33*, 1162−9.
(159) Jeong, B.; Bae, Y. H.; Lee, D. S.; Kim, S. W. Biodegradable block copolymers as injectable drug-delivery systems. *Nature* **1997**, *388*, 860−2.
(160) Fukukawa, K.; Rossin, R.; Hagooly, A.; Pressly, E. D.; Hunt, J. N.; Messmore, B. W.; Wooley, K. L.; Welch, M. J.; Hawker, C. J. Synthesis and characterization of core-shell star copolymers for in vivo PET imaging applications. *Biomacromolecules* **2008**, *9*, 1329−39.
(161) Yuan, J.; Zhang, H.; Kaur, H.; Oupicky, D.; Peng, F. Synthesis and characterization of theranostic poly(HPMA)-c(RGDyK)-DOTA-^{64}Cu copolymer targeting tumor angiogenesis: tumor localization visualized by positron emission tomography. *Mol. Imaging* **2013**, *12*, 203−12.
(162) Cha, C.; Shin, S. R.; Annabi, N.; Dokmeci, M. R.; Khademhosseini, A. Carbon-based nanomaterials: multifunctional materials for biomedical engineering. *ACS Nano* **2013**, *7*, 2891−7.
(163) Iijima, S.; Ichihashi, T. Single-shell carbon nanotubes of 1-nm diameter. *Nature* **1993**, *363*, 603−5.
(164) Gong, H.; Peng, R.; Liu, Z. Carbon nanotubes for biomedical imaging: the recent advances. *Adv. Drug Delivery Rev.* **2013**, *65*, 1951−63.
(165) Liu, Z.; Cai, W.; He, L.; Nakayama, N.; Chen, K.; Sun, X.; Chen, X.; Dai, H. In vivo biodistribution and highly efficient tumour targeting of carbon nanotubes in mice. *Nat. Nanotechnol.* **2007**, *2*, 47−52.
(166) McDevitt, M. R.; Chattopadhyay, D.; Jaggi, J. S.; Finn, R. D.; Zanzonico, P. B.; Villa, C.; Rey, D.; Mendenhall, J.; Batt, C. A.; Njardarson, J. T.; Scheinberg, D. A. PET imaging of soluble yttrium-86-labeled carbon nanotubes in mice. *PLoS One* **2007**, *2*, e907.
(167) Hong, H.; Yang, K.; Zhang, Y.; Engle, J. W.; Feng, L.; Yang, Y.; Nayak, T. R.; Goel, S.; Bean, J.; Theuer, C. P.; Barnhart, T. E.; Liu, Z.; Cai, W. In vivo targeting and imaging of tumor vasculature with radiolabeled, antibody-conjugated nanographene. *ACS Nano* **2012**, *6*, 2361−70.
(168) Hong, H.; Zhang, Y.; Engle, J. W.; Nayak, T. R.; Theuer, C. P.; Nickles, R. J.; Barnhart, T. E.; Cai, W. In vivo targeting and positron emission tomography imaging of tumor vasculature with ^{66}Ga-labeled nano-graphene. *Biomaterials* **2012**, *33*, 4147−56.
(169) Shi, S.; Yang, K.; Hong, H.; Valdovinos, H. F.; Nayak, T. R.; Zhang, Y.; Theuer, C. P.; Barnhart, T. E.; Liu, Z.; Cai, W. Tumor vasculature targeting and imaging in living mice with reduced graphene oxide. *Biomaterials* **2013**, *34*, 3002−9.
(170) Robinson, J. T.; Tabakman, S. M.; Liang, Y.; Wang, H.; Casalongue, H. S.; Vinh, D.; Dai, H. Ultrasmall reduced graphene oxide with high near-infrared absorbance for photothermal therapy. *J. Am. Chem. Soc.* **2011**, *133*, 6825−31.
(171) Del Vecchio, S.; Zannetti, A.; Fonti, R.; Pace, L.; Salvatore, M. Nuclear imaging in cancer theranostics. *Q. J. Nucl. Med. Mol. Imaging* **2007**, *51*, 152−63.
(172) Baum, R. P.; Kulkarni, H. R. THERANOSTICS: From Molecular Imaging Using Ga-68 Labeled Tracers and PET/CT to Personalized Radionuclide Therapy - The Bad Berka Experience. *Theranostics* **2012**, *2*, 437−47.
(173) Oberg, K. Molecular Imaging Radiotherapy: Theranostics for Personalized Patient Management of Neuroendocrine Tumors (NETs). *Theranostics* **2012**, *2*, 448−58.
(174) Velikyan, I. Molecular imaging and radiotherapy: theranostics for personalized patient management. *Theranostics* **2012**, *2*, 424−6.
(175) Ben-Haim, S.; Ell, P. ^{18}F-FDG PET and PET/CT in the evaluation of cancer treatment response. *J. Nucl. Med.* **2009**, *50*, 88−99.
(176) Hess, S.; Blomberg, B. A.; Zhu, H. J.; Hoilund-Carlsen, P. F.; Alavi, A. The Pivotal Role of FDG-PET/CT in Modern Medicine. *Acad. Radiol.* **2014**, *21*, 232−49.
(177) Coenen, H. H.; Elsinga, P. H.; Iwata, R.; Kilbourn, M. R.; Pillai, M. R.; Rajan, M. G.; Wagner, H. N., Jr.; Zaknun, J. J. Fluorine-18 radiopharmaceuticals beyond [^{18}F]FDG for use in oncology and neurosciences. *Nucl. Med. Biol.* **2010**, *37*, 727−40.
(178) Cole, E. L.; Stewart, M. N.; Littich, R.; Hoareau, R.; Scott, P. J. Radiosyntheses Using Fluorine-18: the Art and Science of Late Stage Fluorination. *Curr. Top. Med. Chem.* **2014**, *14*, 875−900.
(179) Groheux, D.; Espie, M.; Giacchetti, S.; Hindie, E. Performance of FDG PET/CT in the clinical management of breast cancer. *Radiology* **2013**, *266*, 388−405.
(180) Li, D.; Lu, P. X. Application of fluorine-18 fluorodeoxyglucose-positron emission tomography and positron emission tomography computed tomography in patients with tuberculosis. *Zhonghua Jiehe He Huxi Zazhi* **2012**, *35*, 852−4.
(181) Alauddin, M. M. Positron emission tomography (PET) imaging with ^{18}F-based radiotracers. *Am. J. Nucl. Med. Mol. Imaging* **2012**, *2*, 55−76.
(182) Caldarella, C.; Isgro, M. A.; Treglia, I.; Treglia, G. Is fluorine-18-fluorodeoxyglucose positron emission tomography useful in monitoring the response to treatment in patients with multiple myeloma? *Int. J. Hematol.* **2012**, *96*, 685−91.
(183) Morgat, C.; Hindie, E.; Mishra, A. K.; Allard, M.; Fernandez, P. Gallium-68: chemistry and radiolabeled peptides exploring different oncogenic pathways. *Cancer Biother. Radiopharm.* **2013**, *28*, 85−97.
(184) Rosch, F. Past, present and future of ^{68}Ge/^{68}Ga generators. *Appl. Radiat. Isot.* **2013**, *76*, 24−30.
(185) Breeman, W. A.; de Blois, E.; Sze Chan, H.; Konijnenberg, M.; Kwekkeboom, D. J.; Krenning, E. P. ^{68}Ga-labeled DOTA-peptides and ^{68}Ga-labeled radiopharmaceuticals for positron emission tomography: current status of research, clinical applications, and future perspectives. *Semin. Nucl. Med.* **2011**, *41*, 314−21.
(186) Banerjee, S. R.; Pomper, M. G. Clinical applications of Gallium-68. *Appl. Radiat. Isot.* **2013**, *76*, 2−13.
(187) Basu, S.; Kumar, R.; Rubello, D.; Fanti, S.; Alavi, A. PET imaging in neuroendocrine tumors: current status and future prospects. *Minerva Endocrinol.* **2008**, *33*, 257−75.
(188) Kaemmerer, D.; Prasad, V.; Daffner, W.; Haugvik, S. P.; Senftleben, S.; Baum, R. P.; Hommann, M. Radioguided surgery in neuroendocrine tumors using Ga-68-labeled somatostatin analogs: a pilot study. *Clin. Nucl. Med.* **2012**, *37*, 142−7.
(189) Win, Z.; Al-Nahhas, A.; Rubello, D.; Gross, M. D. Somatostatin receptor PET imaging with Gallium-68 labeled peptides. *Q. J. Nucl. Med. Mol. Imaging* **2007**, *51*, 244−50.
(190) Gains, J. E.; Bomanji, J. B.; Fersht, N. L.; Sullivan, T.; D'Souza, D.; Sullivan, K. P.; Aldridge, M.; Waddington, W.; Gaze, M. N. ^{177}Lu-DOTATATE molecular radiotherapy for childhood neuroblastoma. *J. Nucl. Med.* **2011**, *52*, 1041−7.
(191) Budiawan, H.; Salavati, A.; Kulkarni, H. R.; Baum, R. P. Peptide receptor radionuclide therapy of treatment-refractory metastatic

thyroid cancer using ^{90}Yttrium and ^{177}Lutetium labeled somatostatin analogs: toxicity, response and survival analysis. *Am. J. Nucl. Med. Mol. Imaging* **2013**, *4*, 39−52.
(192) Strigari, L.; Sciuto, R.; Rea, S.; Carpanese, L.; Pizzi, G.; Soriani, A.; Iaccarino, G.; Benassi, M.; Ettorre, G. M.; Maini, C. L. Efficacy and toxicity related to treatment of hepatocellular carcinoma with ^{90}Y-SIR spheres: radiobiologic considerations. *J. Nucl. Med.* **2010**, *51*, 1377−85.
(193) Wu, S.-Y.; Chang, T.-K.; Kuo, J.-W.; Liu, R.-S.; Wang, H.-E. Evaluation of ^{68}Ga/^{111}In-SIR-Spheres as a novel PET/SPECT imaging surrogate of ^{90}Y-SIR-Spheres. *J. Nucl. Med.* **2010**, *51* (S2), 1553.
(194) Avila-Rodriguez, M. A.; Selwyn, R. G.; Hampel, J. A.; Thomadsen, B. R.; Dejesus, O. T.; Converse, A. K.; Nickles, R. J. Positron-emitting resin microspheres as surrogates of ^{90}Y SIR-Spheres: a radiolabeling and stability study. *Nucl. Med. Biol.* **2007**, *34*, 585−90.
(195) Capala, J.; Bouchelouche, K. Molecular imaging of HER2-positive breast cancer: a step toward an individualized 'image and treat' strategy. *Curr. Opin. Oncol.* **2010**, *22*, 559−66.
(196) Jacob, J.; Kirova, Y. M. Locoregional breast radiotherapy and concurrent treatment with trastuzumab. *Bull. Cancer* **2014**, *101*, 40−51.
(197) Stipsanelli, E.; Valsamaki, P. Monoclonal antibodies: old and new trends in breast cancer imaging and therapeutic approach. *Hell J. Nucl. Med.* **2005**, *8*, 103−8.
(198) Dijkers, E. C.; Oude Munnink, T. H.; Kosterink, J. G.; Brouwers, A. H.; Jager, P. L.; de Jong, J. R.; van Dongen, G. A.; Schroder, C. P.; Lub-de Hooge, M. N.; de Vries, E. G. Biodistribution of ^{89}Zr-trastuzumab and PET imaging of HER2-positive lesions in patients with metastatic breast cancer. *Clin. Pharmacol. Ther.* **2010**, *87*, 586−92.
(199) Bourgeois, A. C.; Chang, T. T.; Fish, L. M.; Bradley, Y. C. Positron emission tomography/computed tomography in melanoma. *Radiol. Clin. North Am.* **2013**, *51*, 865−79.
(200) Brunetti, J. PET/CT in gynecologic malignancies. *Radiol. Clin. North Am.* **2013**, *51*, 895−911.
(201) Bunevicius, A.; Yuan, H.; Lin, W. The potential roles of ^{18}F-FDG-PET in management of acute stroke patients. *Biomed. Res. Int.* **2013**, DOI: 10.1155/2013/634598.
(202) Elsinga, P. H.; Dierckx, R. A. Small Molecule PET-Radiopharmaceuticals. *Curr. Pharm. Des* **2014**, *20*, 2268−74.
(203) Escott, E. J. Role of positron emission tomography/computed tomography (PET/CT) in head and neck cancer. *Radiol. Clin. North Am.* **2013**, *51*, 881−93.
(204) Fischer, G.; Seibold, U.; Schirrmacher, R. Wangler, B.; Wangler, C. ^{89}Zr, a radiometal nuclide with high potential for molecular imaging with PET: chemistry, applications and remaining challenges. *Molecules* **2013**, *18*, 6469−90.
(205) Fularz, M.; Adamiak, P.; Czepczynski, R.; Jarzabek-Bielecka, G.; Kedzia, W.; Ruchala, M. Positron emission tomography (PET) in malignant ovarian tumors. *Ginekol. Pol.* **2013**, *84*, 720−5.
(206) Hinds, S. R., 2nd; Stocker, D. J.; Bradley, Y. C. Role of positron emission tomography/computed tomography in dementia. *Radiol. Clin. North Am.* **2013**, *51*, 927−34.
(207) Jadvar, H. Molecular imaging of prostate cancer with PET. *J. Nucl. Med.* **2013**, *54*, 1685−8.
(208) Lecouvet, F. E.; Lhommel, R.; Pasoglou, V.; Larbi, A.; Jamar, F.; Tombal, B. Novel imaging techniques reshape the landscape in high-risk prostate cancers. *Curr. Opin. Urol.* **2013**, *23*, 323−30.
(209) Mirpour, S.; Mhlanga, J. C.; Logeswaran, P.; Russo, G.; Mercier, G.; Subramaniam, R. M. The role of PET/CT in the management of cervical cancer. *AJR, Am. J. Roentgenol* **2013**, *201*, W192−205.
(210) Nemeth, Z.; Boer, K.; Kasler, M.; Borbely, K. Clinical use of ^{18}F-FDG PET/CT in colorectal carcinoma. *Orv. Hetil.* **2013**, *154*, 1447−53.
(211) Notaristefano, A.; Niccoli Asabella, A.; Stabile Ianora, A. A.; Merenda, N.; Moschetta, M.; Antonica, F.; Altini, C.; Ferrari, C.; Cesarano, E.; Rubini, G. ^{18}F-FDG PET/CT in staging and restaging cholangiocarcinoma. *Recenti Prog. Med.* **2013**, *104*, 328−35.
(212) Ouvrier, M. J.; Vignot, S.; Thariat, J. State of the art in nuclear imaging for the diagnosis of bone metastases. *Bull. Cancer* **2013**, *100*, 1115−24.
(213) Shreve, P.; Faasse, T. Role of positron emission tomography-computed tomography in pulmonary neoplasms. *Radiol. Clin. North Am.* **2013**, *51*, 767−79.
(214) Velikyan, I. Prospective of Ga-Radiopharmaceutical Development. *Theranostics* **2013**, *4*, 47−80.
(215) Viswanathan, C.; Bhosale, P. R.; Shah, S. N.; Vikram, R. Positron emission tomography-computed tomography imaging for malignancies in women. *Radiol. Clin. North Am.* **2013**, *51*, 1111−25.
(216) Wang, L.; Tang, K.; Zhang, Q.; Li, H.; Wen, Z.; Zhang, H.; Zhang, H. Somatostatin receptor-based molecular imaging and therapy for neuroendocrine tumors. *Biomed. Res. Int.* **2013**, *2013*, 102819.
(217) Wright, B. D.; Lapi, S. E. Designing the magic bullet? The advancement of immuno-PET into clinical use. *J. Nucl. Med.* **2013**, *54*, 1171−4.
(218) Holland, J. P.; Williamson, M. J.; Lewis, J. S. Unconventional nuclides for radiopharmaceuticals. *Mol. Imaging* **2010**, *9*, 1−20.
(219) Huang, J.; Cui, L.; Wang, F.; Liu, Z. PET tracers based on ^{86}Y. *Curr. Radiopharm.* **2011**, *4*, 122−30.
(220) Bourgeois, M.; Rajerison, H.; Guerard, F.; Mougin-Degraef, M.; Barbet, J.; Michel, N.; Cherel, M.; Faivre-Chauvet, A. Contribution of [^{64}Cu]-ATSM PET in molecular imaging of tumour hypoxia compared to classical [18F]-MISO–a selected review. *Nucl. Med. Rev. Cent. East. Eur.* **2011**, *14*, 90−5.
(221) Vavere, A. L.; Rossin, R. Molecular imaging of cancer with radiolabeled peptides and PET. *Anticancer Agents Med. Chem.* **2012**, *12*, 462−75.
(222) Welch, M. J.; Laforest, R.; Lewis, J. S. Production of non-standard PET radionuclides and the application of radiopharmaceuticals labeled with these nuclides. *Ernst Schering Res. Found. Workshop* **2007**, 159−81.
(223) Deri, M. A.; Zeglis, B. M.; Francesconi, L. C.; Lewis, J. S. PET imaging with ^{89}Zr: from radiochemistry to the clinic. *Nucl. Med. Biol.* **2013**, *40*, 3−14.
(224) Urruticoechea, A.; Alemany, R.; Balart, J.; Villanueva, A.; Vinals, F. Capella, G. Recent advances in cancer therapy: an overview. *Curr. Pharm. Des.* **2010**, *16*, 3−10.
(225) Riehemann, K.; Schneider, S. W.; Luger, T. A.; Godin, B.; Ferrari, M.; Fuchs, H. Nanomedicine–challenge and perspectives. *Angew. Chem., Int. Ed.* **2009**, *48*, 872−97.
(226) Sanhai, W. R.; Sakamoto, J. H.; Canady, R.; Ferrari, M. Seven challenges for nanomedicine. *Nat. Nanotechnol.* **2008**, *3*, 242−4.
(227) Lanza, G. M.; Moonen, C.; Baker, J. R., Jr.; Chang, E.; Cheng, Z.; Grodzinski, P.; Ferrara, K.; Hynynen, K.; Kelloff, G.; Lee, Y. E.; Patri, A. K.; Sept, D.; Schnitzer, J. E.; Wood, B. J.; Zhang, M.; Zheng, G.; Farahani, K. Assessing the barriers to image-guided drug delivery. *Wiley Interdiscip. Rev.: Nanomed. Nanobiotechnol.* **2014**, *6*, 1−14.